Analysis of atmospheric CO2 variability in the Marseille city area and the north-west Mediterranean basin at different time scales

Irène Xueref-Remy, Mélissa Milne, Narimène Zoghbi, Ludovic Lelandais, Aurélie Riandet, Alexandre Armengaud, Ludovic Lanzi, Grégory Gille, Sonia Oppo, Lola Brégonzio-Rozier, et al.

ATMOSPHERIC ENVIRONMENT: X 17 (2023) 100208

Contents lists available at ScienceDirect

Atmospheric Environment: X

journal homepage: www.journals.elsevier.com/atmospheric-environment-x

Analysis of atmospheric CO_2 variability in the Marseille city area and the north-west Mediterranean basin at different time scales

Irène Xueref-Remy [a,b,*,1,2], Mélissa Milne [b,1,2], Narimène Zoghbi [b,1], Ludovic Lelandais [a], Aurélie Riandet [a], Alexandre Armengaud [c], Grégory Gille [c], Ludovic Lanzi [c], Sonia Oppo [c], Lola Brégonzio-Rozier [d,1], Pierre-Eric Blanc [e], Christophe Yohia [f], Jacques Piazzola [b], Marc Delmotte [d]

[a] Aix Marseille Univ, Avignon Université, CNRS, IRD, IMBE (Institut Méditerranéen de Biodiversité et d'Ecologie marine et continentale), Aix, Marseille, France
[b] MIO (Mediterranean Institute of Oceanography), CNRS, Marseille, France
[c] ATMOSUD (Observatoire de la qualité de l'air en région SUD Provence-Alpes-Côte d'Azur), Marseille, France
[d] LSCE (Laboratoire des Sciences du Climat et de l'Environnement), Gif-sur-Yvette, France
[e] OHP (Observatoire de Haute Provence), OSU Institut PYTHEAS, CNRS, Saint-Michel-l'Observatoire, France
[f] OSU Institut PYTHEAS, Service Informatique Pytheas, Marseille, France

ARTICLE INFO

Keywords:
Carbon dioxide
Atmospheric CO_2 variability
Urban emissions
Natural fluxes
Growth rate
Diurnal cycle
Seasonal cycle
Atmospheric dynamics
Meteorology

ABSTRACT

This study presents the first analysis of the variability of atmospheric CO_2 in the area of the Marseille city (France). It addresses the role of anthropogenic emissions, natural fluxes and atmospheric boundary layer height (ABLH) dynamics on CO_2 variability at the diurnal, synoptic, seasonal and multi-annual scales. A regional network based on 4 in-situ observation sites of CO_2, CO and NOx was deployed between 2013 and 2018. One urban site (CAV) located in Marseille center was set up in collaboration with the regional air quality monitoring agency ATMOSUD. A second site (SME) was installed at the coastal edge of Marseille at the border of the Mediterranean Sea. The two other sites belonging to the ICOS (integrated Carbon Observing System) national atmospheric greenhouse observation network, are located in natural areas at the Observatoire de Haute Provence (OHP, 80 km north of Marseille) and at Cape Corsica (ERSA, 330 km east of Marseille) and are defined as regional background sites. The comparison between the sites was performed on the period common to all sites (1 July 2016–13 February 2018). The datasets are calibrated on the reference World Meteorological Organization scales for CO_2 and CO with high precision and accuracy levels. At all sites, the mean annual CO_2 growth rate is found to be quite similar to the Mauna Loa (Hawaii) reference site one, but mean annual CO_2 concentrations are higher of several ppm at both urban sites than at both background sites. The diurnal cycle shows a higher amplitude at the urban sites (14.5 ppm at SME; 18.8 ppm at CAV) than at the background sites (5.3 ppm at OHP; 0.5 ppm at ERSA), as in other urban studies. While the urban stations are influenced by large urban anthropogenic emissions (mostly from traffic and heating, especially in winter), both background sites are mainly influenced by natural fluxes. At ERSA, the CO_2 diurnal cycle is found to be primarily controlled by the small air-sea CO_2 fluxes. At OHP, the diurnal variability of CO_2 is mainly driven by the activity of vegetation (photosynthesis and respiration) and ABLH dynamics. For similar reasons, atmospheric CO_2 concentrations are also characterized by larger seasonal variations in the city (29.2 ppm at CAV and 20.3 ppm at SME, respectively) than at OHP (13.1 ppm) and at SME (13.9 ppm). The influence of local, regional and remote anthropogenic emissions is assessed through a classification of the datasets by wind conditions. Similarly to other urban studies, a dome of several tens of ppm of CO_2 gets formed over the city at low wind speed (less than 4 m s^{-1}). For higher wind speeds (4–10 m s^{-1}), the influence of regional and remote emissions on atmospheric CO_2 is function of wind direction, varying from a few ppm at the background sites to a plume of more than 10 ppm at the urban ones. For very strong winds, the CO_2 plume gets diluted. Finally local breezes, although not much frequent and more occurrent in summer, partly

* Corresponding author. Aix Marseille Univ, Avignon Université, CNRS, IRD, IMBE (Institut Méditerranéen de Biodiversité et d'Ecologie marine et continentale), Aix, Marseille, France.
E-mail address: irene.remy-xueref@univ-amu.fr (I. Xueref-Remy).
[1] Formerly at (relates to number that follows).
[2] These authors contributed equally to this work.

https://doi.org/10.1016/j.aeaoa.2023.100208
Received 3 November 2022; Received in revised form 7 February 2023; Accepted 9 February 2023
Available online 14 February 2023

control atmospheric CO_2 concentrations in Marseille. Additional local meteorological measurement sites would help to better characterize breezes in Marseille. Also, our study shows that additional background sites closer to the city on the path of the dominant winds would help to better constrain Marseille CO_2 urban dome and plume. The NW and W sectors show a higher CO_2 concentration variability even for strong winds, with likely an impact of the industrial area of Fos-Berre north-west of Marseille. Furthermore, as CO and NOx are used to assess the role of anthropogenic emissions vs natural fluxes on CO_2, future dedicated campaigns using carbon isotopes will help to decipher the role of fossil fuel combustion sources vs modern ones on CO_2 in Marseille. Finally, remote sensing measurements would be useful to better assess the impact of ABLH on atmospheric CO_2 in the coastal area of Marseille where atmospheric dynamics are quite complex.

1. Introduction

Since the industrial revolution, the concentration of atmospheric greenhouse gases has increased exponentially because of the rising release of anthropogenic emissions in the atmosphere, mostly under the form of carbon dioxide (CO_2) (IEA, 2017). This increase is very likely the cause of global climate changes observed over the last decades, which impact the functioning of the environment and of living ecosystems (IPCC et al., 2013; IPCC et al., 2021). The main source of anthropogenic CO_2 is the combustion of fossil fuels (FF), accounting for about 86% of global CO_2 emissions on the 2010–2019 decade (Friedlingstein et al., 2020). More than 70% of $FFCO_2$ emissions are estimated to come from urbanized and industrialized areas (Seto et al., 2014). However, there are still large uncertainties on their regional distribution and partition by emission sectors as given by the bottom-up estimates of emission inventories (Rayner et al., 2010). Hence, over the last years there has been a growing interest to verify CO_2 emissions from urban centers and their associated industrial facilities through atmospheric top-down approaches, that combine both atmospheric measurements and atmospheric transport modelling, e.g. in Indianapolis (e.g. Turnbull et al., 2018), Los Angeles megacity (e.g. Verhulst et al., 2017), Paris megacity (e.g. Bréon et al., 2015; Ammoura et al., 2016; Staufer et al., 2016; Xueref-Remy et al., 2018) and the Washington DC–Baltimore Metropolitan Area (e.g. Martin et al., 2019). These studies revealed that local urban CO_2 emissions create either an urban CO_2 dome over the city or a plume downwind of the city, with CO_2 concentrations higher of a few parts per million (ppm) to several tens of ppm than those encountered in surrounding areas when these areas are not exposed to the urban plume (hence defined as background concentrations). These studies also revealed how atmospheric CO_2 variability is complex in these areas and they inferred the different factors that control it, mainly: 1/the vicinity of the observing site to local CO_2 sources and sinks and the nature/-strength of those, 2/the advection of remote CO_2 fluxes in the area of study, 3/meteorological conditions (mostly wind speed, wind direction and temperature) and 4/atmospheric boundary layer dynamics (Idso et al., 2001; Nasrallah et al., 2003; Gratani and Varone, 2005; Rice and Bostrom, 2011; Turnbull et al., 2015; Xueref-Remy et al., 2018). These projects also provided independent assessments of regional bottom-up CO_2 emission inventories through the use of top-down approaches. The latters include: 1/correlations studies between CO_2 and emission tracers i.e. species co-emitted with CO_2 during combustion processes, such as carbon monoxide (CO) used as a tracer of incomplete combustion processes (e.g. Ammoura et al., 2016), nitrogen oxides (NOx) used as a tracer of traffic (e.g. Lopez et al., 2013) and carbon isotopes used to trace biogenic vs FFCO2 fluxes (e.g. Turnbull et al., 2015); and 2/atmospheric inverse transport modelling, that ideally requires continuous atmospheric CO_2 measurements on urban, peri-urban and rural/remote sites to assess the CO_2 urban plume by calculating the gradient between pairs of upwind and downwind sites of the city within a cone of wind direction, generally of the order of 30° (e.g. Bréon et al., 2015; Lauvaux et al., 2016; Nathan et al., 2018; Staufer et al., 2016; Lopez-Coto et al., 2020).

Today, more than half of the global population leaves in cities and urbanization is forecast to grow fast over the next decades (United Nations, 2019). Without any efforts in mitigating our emissions, this may increase the contribution of cities and their industrial facilities to global anthropogenic CO_2 emissions (Wolf et al., 2011; Ritchie and Roser, 2020). Only decisions of emissions mitigation, carbon storage and green technologies will bring to the reduction of anthropogenic CO_2 emissions, especially within the framework of regional climate plans for the hotspots of CO_2 emissions that constitute cities and industries. But to define efficient regional pathways, it is first necessary to reduce the uncertainties on the emission estimates of anthropized regions.

Some regions of the world are more exposed to the risks of climate change, such as the Mediterranean Basin (IPCC et al., 2013; IPCC et al., 2021). Furthermore, urban centers are exposed to higher temperatures than peri-urban and rural or marine surroundings due to the urban heat island effect (e.g. Pal et al., 2012; Lac et al., 2013): this makes urbanized areas even more exposed to the risks of climate change. The SUD Provence-Alpes-Côte d'Azur (SUD-PACA) Region in the south-east of France is much exposed to climate change and is much urbanized. Especially, this region comprises the Aix-Marseille-Provence metropolis (1.8 million inhabitants) located on the north-west coast of the Mediterranean Sea. This metropolis is the second most populated area of France after the Paris megacity, accounting for 37% of the population of the SUD-PACA region. According to ATMOSUD (Agency for Air Quality Monitoring in the SUD-PACA region), the SUD-PACA emissions are estimated to represent about 10% of national CO_2 emissions (https://www.atmosud.org/sites/paca/files/atoms/files/180000_oreca_bilan_2018_net.pdf) and the Aix-Marseille Metropolis emits more than one half of the regional emissions (22.9 Mt of CO_2 in 2019: cigale.atmosud.org). Industrial activities (energy sector excluded) are the main emitting sector (60%), followed by road traffic (15%), energy production and distribution (10%), residential and office activities including heating (8%), maritime and aerial transport (3%), waste treatment (1%) and other minor emitters (3%). However, the emission estimates delivered by ATMOSUD are based on the product of bench-marked emission factors that can quite be different from real condition ones. Top-down approaches that can assess independently these estimates are thus required to reduce the uncertainties of these latters.

The first step of top-down approaches is to assess whether one can detect an increase in atmospheric CO_2 concentration over and downwind of the urbanized/industrialized area due to local/regional emissions as compared to regional background concentrations, and how this increase varies at different time scales. As mention above, atmospheric CO_2 is controlled by several factors, which for the Aix-Marseille-Provence area comprise CO_2 emissions and sinks (continental and marine ones) at the local, regional, continental and global scales, as well as advection and boundary layer dynamics (e.g. Xueref-Remy et al., 2018; Conil et al., 2019). These factors vary at the hourly, diurnal, synoptic, seasonal and interannual scales which have to be taken into account to understand the variability of atmospheric CO_2.

In this framework, the Aix-Marseille Carbon project (AMC, 2016–2019) was set-up to develop a first top-down pilot study on assessing the impact of anthropogenic CO_2 emissions on atmospheric CO_2 on the coastal Aix-Marseille-Provence metropolis area. In this purpose and in collaboration with the national ICOS (Integrated Carbon Observing System) France atmospheric greenhouse observation network

(Delmotte et al., 2015), a regional atmospheric network of 4 in-situ CO_2 observing stations was developed along a rural, urban, coastal and marine gradient in and around the Aix-Marseille area (the urban and coastal sites being in Marseille city) to collect data during at least 1.5 year at each site between April 2013 and February 2018. Based on these datasets, this work presents an analysis of the spatio-temporal variability of atmospheric CO_2 at the hourly to the seasonal scales in the south-east of France and north-west Mediterranean basin, which has never been studied earlier. The Aix-Marseille-Provence metropolis is settled on a rough landscape made of valleys and hills, which height varies between 300 and 800 m (François et al., 2005; Mestayer et al., 2005; Puygrenier et al., 2005). This complex topography, combined to the proximity of the Mediterranean Sea, generates local to regional sea/land breeze regimes and a strong regional wind called Mistral (Mestayer et al., 2005; Puygrenier et al., 2005). To our knowledge, there has been only a few atmospheric field studies in coastal cities which assessed the role of breezes on modulating atmospheric CO_2 concentration (e.g. Verhulst et al., 2017) and usually on relatively short time scales (e.g. Pérez-Landa et al., 2007; Mahesh et al., 2014). This work presents for the first time an analysis of atmospheric CO_2 in a coastal city of the Mediterranean Basin and in France on a time scale larger than 1.5 years.

In the following, Section 2 introduces the observation sites, the instrumentation and the datasets that were developed and used to conduct this work. Section 3 presents the analysis of atmospheric CO_2 at different timescales on the area of interest from June 2016 to February 2018 and a discussion on the results. Section 4 gives the conclusion of this study and presents the main perspectives of this work.

2. Material and methods

2.1. Observing sites

Within the AMC (Aix-Marseille Carbon Pilot Study) project funded by the Aix-Marseille LABEX OT-MED, continuous measurements of atmospheric CO_2 were carried out at four sites in the SUD-PACA region and north-west Mediterranean Sea on a rural, urban, coastal and marine gradient (Fig. 1 and Table 1). The environment of each site is illustrated in Fig. 2. The urban site (CAV) was installed in the center of Marseille, which is the most populated area of the Aix-Marseille-Provence metropolis. Another site (SME) was installed at the coastal edge of Marseille and of the Mediterranean Sea to study the impact of the land-sea breeze process on atmospheric CO_2 variability. Two ICOS-France sites (OHP and ERSA) were used as regional background sites to infer the urban CO_2 plume of Marseille city from the CAV and SME datasets. Depending on each station, measurements started between April 2013 and July 2016. The corresponding timeseries analyzed in this study run until 13 February 2018 for CAV, SME and OHP, and until 13 December 2017 for ERSA (an instrumental failure occurred at that site afterwards). At the four sites, the instrumentation was equipped with calibration tanks linked to the international WMO/CO_2 scale, as explained further.

The CAV site is located in Marseille city center and is part of the ATMOSUD regional air quality monitory network (https://www.atmosud.org/fiche-station/marseille-longchamp). Atmospheric CO_2 measurements began at CAV in July 2016. ATMOSUD provided the raw CO_2 measurements and IMBE performed the data calibration and quality control (see Section 2.2). CAV is located in the 4th district of Marseille

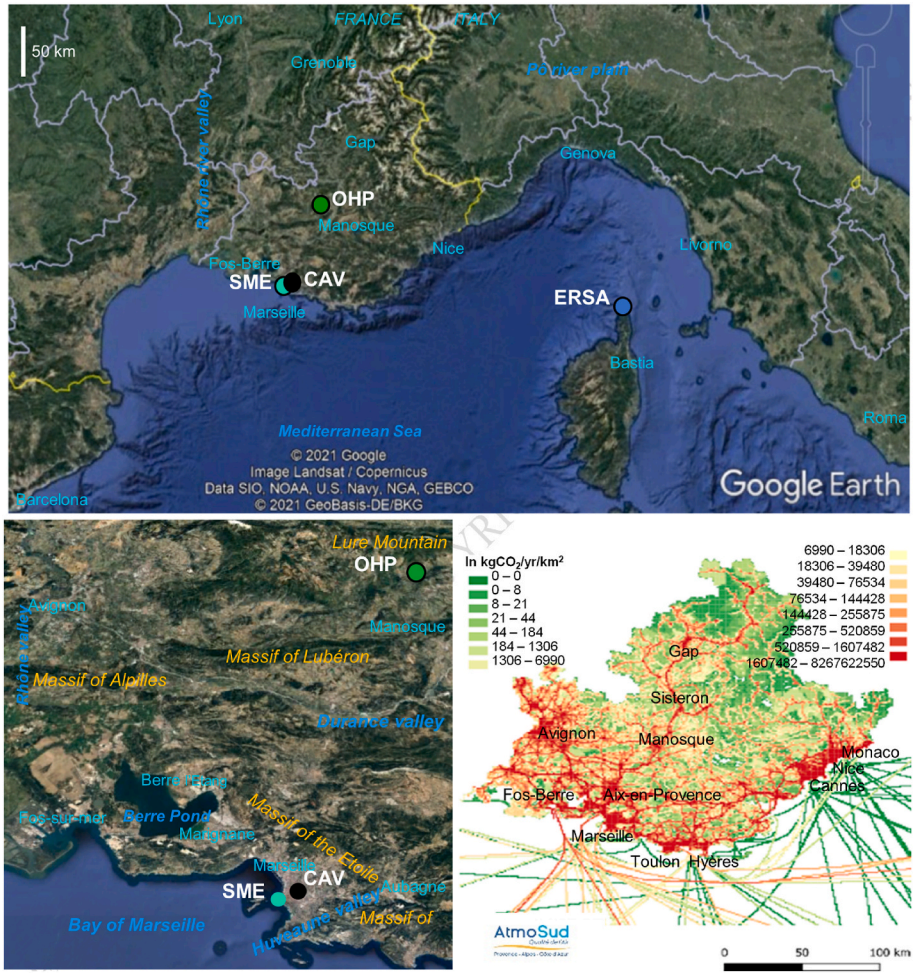

Fig. 1. Top: Map showing the location of the four CO_2 observing stations of this study (CAV, SME, OHP and ERSA) in the region of Aix-Marseille-Provence metropolis (SUD-PACA region, FRANCE) and in the North-West Mediterranean Sea area (light blue: cities; italic dark blue: natural water features; light orange: hills and mountains areas). Bottom left: zoom on the three stations located in the Sud-PACA region (CAV, SME and OHP). Bottom right: Annual spatialized bottom-up CO_2 emission estimates (in $kgCO_2$/year/km) in the SUD-PACA region for the year 2013 (source: ATMOSUD, personal communication). (For interpretation of the references to colour in this figure legend, the reader is referred to the Web version of this article.)

Table 1
Atmospheric CO_2 observation sites information (ASL = Above Sea Level; AGL = Above Ground Level).

Site	Location	Latitude (deg. N)	Longitude (deg. E)	Type	Elevation (m ASL)	Sampling height (m AGL)
CAV	Marseille (center)	43.3059	5.3950	Urban	65	5
SME	Marseille (coast)	43.2806	5.3499	Coastal urban	10	2.5
OHP	St-Michel-l'Observatoire	43.9315	5.7134	Rural	650	10, 50, 100
ERSA	Cape Corsica	42.9914	9.3798	Marine	530	40

Fig. 2. The four observation sites in their environment (top left: CAV, bottom left: SME, bottom right: OHP ICOS tower, top right: ERSA ICOS tower).

city, 64 m above sea level (ASL). The sampling height is 5 m above ground level (AGL). In the 90–270° (East to West) sector of the sation, the Marseille Longchamp Park - mostly covered by trees and grasses - spreads over approximatively 7 Ha. CAV is largely exposed to urban emissions and is defined as an urban site.

The SME site (Station Marine d'Endoume) belongs to IMBE. Atmospheric CO_2 measurements were launched at SME in July 2016 within the AMC project. SME is located on the coast of Marseille, at the western point of the city (which is orientated North to South). During this study, air was sampled from an inlet fixed on a 2.5 m mast settled on the roof of a 20 m building at the seashore. The 180-0° sector of SME is the bay of Marseille in the Mediterranean Sea, while the 0–180° sector is strongly urbanized. Located at the edge of the city, SME is classified as a coastal urban station due to its proximity to the Mediterranean Sea in an urban environment.

The OHP station is located at the Observatoire de Haute Provence, about 80 km north of the center of Marseille. It belongs to the ICOS-France national atmospheric greenhouse gases network (Delmotte et al., 2015). This station is operational since July 2014. The measurements are collected at three sampling levels: 10 m, 50 m and 100 m AGL (Lelandais et al., 2022). OHP is settled in a white oak trees wood and is further surrounded by pastures and cultivated fields, and a few villages and cities. The closest village located 3 km away in the southern direction is Saint-Michel l'Observatoire (about 1140 inhabitants), and the closest cities are Forcalquier and Manosque (about 5000 and 22000 inhabitants, resp.) located 10 km NE and 16 km SE, resp.. The closest highway is about 20 km away from OHP (A51, oriented NE-SW). OHP is classified as a rural site and it is here used to assess the atmospheric CO_2 rural background concentrations i.e. the CO_2 concentration in the region of Aix-Marseille metropolis, as OHP is only subject to a low influence of emissions from this latter (Lelandais et al., 2022).

The ERSA station is located at Cape Corsica, approximately 330 km east of Marseille city. It is located in the extreme north of Corsica, at an altitude of 530 m ASL, about 50 km north of Bastia. This site is operational since April 2013 and belongs to the ICOS-France network like OHP. The air inlet is set up on top of a tower at 40 m AGL. ERSA is classified as a marine background site and is used to assess the regional atmospheric CO_2 marine background concentration i.e. the CO_2 concentration in the marine sector of the Aix-Marseille-Provence metropolis without the influence of the emissions from this latter.

2.2. Instrumentation

The CO_2 datasets were continuously collected with a time step of 5 s at each station on the time periods given in Table 2, using CRDS (Cavity Ring Down Spectroscopy) analyzers. Three of these analysers were also monitoring atmospheric CO (carbon monoxide), a useful tracer of uncomplete combustion processes, at OHP, SME et ERSA (PICARRO G2401 model) sites. At CAV, the CRDS analyser was not monitoring CO

Table 2
Instrumentation, period and resolution of the measurements and species recorded at each site.

Station	Analyser type	Sampling period	Resolution (s)	Species
CAV	Picarro G2301 + Environnement SA ACM32	01 July 2016 to 13 February 2018	5	CO_2, NOx
SME	Picarro G2401	01 July 2016 to 13 February 2018	5	CO_2, CO
OHP	Picarro G2401	16 July 2014 to 13 February 2018	5	CO_2, CO
ERSA	Picarro G2401	25 April 2013 to 13 December 2017	5	CO_2, CO

(PICARRO G2301 model), but other tracers of combustion typical of traffic (nitrogen oxides, NO_X) were monitored continuously by ATMOSUD using a chemiluminescence analyser (ENVIRONNEMENT SA AC32M model). The uncertainty of the NOx hourly dataset used in this study is less than 11.5% (ATMOSUD, personal communication).

The CRDS analyzer worked continuously at a flow rate of 150 mL min^{-1} to pump air through a Synflex® ¼ inch line. Filters (cutoff diameters: 2 μm and 0.5 μm) were placed at the entrance of the air inlet to trap anthropogenic and natural particles (dust, sea salt …) in order to protect the instrumentation parts from particle deposition. The sampling cell of the PICARRO CRDS analyzers was automatically regulated in temperature (45 °C) and pressure (140 Torr). During the quality control process, the CO_2 and CO datasets were filtered in temperature and pressure according to the ICOS procedure (Hazan et al., 2016): only the data respecting the ICOS thresholds ($T = 45 \pm 0.004$ °C et $P = 140 \pm 0.1$ Torr) have been kept for our scientific analysis. Following PICARRO and ICOS procedures, a correction on the CO_2 concentration function of the atmospheric water vapor content was performed automatically by the ICOS database for the OHP and ERSA datasets (Hazan et al., 2016) and by the analyzer PICARRO software for the CAV and SME ones (Rella et al., 2010). Furthermore, data related to local perturbations, such as human respiration during maintenance operations, were removed manually. After these two filtering processes, more than 95% of the raw datasets were validated. Each station was equipped with calibration tanks (two to four tanks depending on the site and on periods) containing dry compressed air at different CO_2 and CO concentrations ranging from 380 to 500 ppm for CO_2 and from 80 to 200 ppb for CO. Before their deployment, these tanks were calibrated at LSCE on the WMO X-2007 scale for CO_2 and X-2004 scale for CO (Lopez et al., 2012). The tanks and the air inlet were connected to the CRDS analyser using an automatic gas distribution box. The calibration sequence was run each 30 days and comprised three cycles. Each cycle consisted in analyzing the tanks' gas concentration one after the other with the CRDS analyzer for 15 min each. Only the last cycle was retained. For each tank, the mean of the last 5 min of the measurements was calculated and attributed as the tank concentration measured by the CRDS analyzer.

The tank CRDS mean values were drawn function of the concentration of the tanks measured on the WMO scale at LSCE to calculate the calibration equation, which has then been applied to the air datasets. One further tank, called "target", was used to calculate the accuracy and precision of the datasets. The target gas was run every 47 h for 15 min. The mean concentration of the target tank was calculated on the last 5 min of these 15 min. The accuracy of the CRDS datasets was calculated as the difference between the average concentration of the target measured on site and the one attributed at LSCE on the WMO scale: it is less than 0.1 ppm (resp. −0.2 ppm) for CO_2 and less than 1 ppb for CO at OHP, ERSA and CAV (resp. SME). The precision of the CRDS datasets, reported as the standard deviation of the onsite target average concentration, is less than 0.1 ppm for CO_2 and less than 11.5 ppb for CO at the four sites.

The CO_2 growth rate values at OHP and ERSA have been calculated using the data comprised between the first and the third quartiles of the datasets, as in Vermeulen et al. (2011). The mean annual values of each subset have been computed. Since there are only 3 full years of data common to OHP and ERSA (2015, 2016, 2017), it was not much relevant to perform a linear regression. The growthrate of CO_2 at each site was rather estimated by substracting the 2016 subset mean to the 2015 subset one and the 2017 subset mean to the 2016 subset one; then, the average and standard deviation of both means were calculated and provided as the growth rate estimate and the growth rate variability at the site, respectively.

2.3. Wind datasets, boundary layer height and backtrajectories

For each station, datasets of wind speed (ws), wind direction (wd) and atmospheric boundary layer height (ABLH) were extracted from 1 July 2016 to 31 January 2018 corresponding to the period when the 4 sites produced data almost all the time (see Table 2), from the regional WRF model (Weather Research and Forecasting) version 3.7 released on 17 April 2015. As there were no validated ABLH WRF data available for the ERSA site on this period for the months of January to March, we extracted additional data from 1 January 2016 to 30 June 2016 to get a full seasonal cycle of the ABLH at all sites (section 3.3). Our domain covers the SUD-PACA region and the North-East Mediterranean Sea (43.78°N, 41.27°S, 9.62°E, 2.90°E). The model framework runs at a 1h and 2 km resolution and is forced by ECMWF meteorological fields (European Centre for Medium-Range Weather Forecasts: https://www.ecmwf.int/fr) at a 3h and 9 km resolution. Regarding the land surface model, the default Noah LSM scheme is used (Chen and Dudhia,79 2001; Tewari et al., 2004). For atmospheric boundary layer physics, the Mellor–Yamada–Nakanishi–Niino Level 2.5-level (MYNN2) TKE scheme was used together with the corresponding built-in urban canopy model and the ABLH was defined as the height at which the TKE falls below a critical value, as detailed in Banks et al. (2016). For this study, the wind datasets were classified in five classes depending on wind speed inspired by the Beaufort scale (Table 3).

Marseille and the SUD-PACA region are characterised by local meteorological features, mostly due to their uneven topography and their proximity to the Mediterranean Sea. Fig. 3 shows the mean wind roses at each site, computed on the 2016–2018 period from our WRF/ECMWF modelling framework wind fields.

In Marseille, two synoptic regimes are dominant: north-westerly (NW) winds, the most occurrent, and south-easterly (SE) winds. Further north inland at OHP, dominant winds blow from the NW sector and from the north-east (NE) one. At ERSA in the north of Corsica, the wind regimes are dominated by the north-west (NW) sector with a stronger influence from the western side, followed closely by the south-west (SW) sector. The NW sector (NNW and WNW) represents about 45% of the winds blowing at CAV and SME in Marseille city and at OHP and 33% at ERSA (Fig. 3). North-westerly winds are cold and dry and often associated with the so-called "Mistral" wind that has been studied within the ESCOMPTE (Expérience sur Site pour COtraindre les Modèles de Pollution atmosphériques et de Transport d'Emission) campaign (e.g. Guenard et al., 2005; Drobinski et al., 2007). Mistral also blows at ERSA in the north of Corsica but rather from the west sector (Jacq et al., 2005), where it mixes with Libeccio wind (SW sector). In the SUD-PACA region, mistral blows at more than 7 m s^{-1} (Grimmond et al., 2004), and thus enters into the medium, strong and very strong wind classes.

The SE sector represents about 25% of the winds at CAV and SME. As the corresponding air masses often arrive from the Mediterranean Sea, south-easterly (SE) winds are sweet and moist, generally strong. The ESE and SSE sectors are predominant (15% at CAV and 22% at SME), but CAV is also under a non negligible influence of eastern winds (approximately 12%). The NE sector counts for about 22% of the wind rose at OHP and ERSA, while it is less present at CAV and SME (about 12%). The SO sector represents about a third (29%) of total winds at ERSA, while it counts for a bit less than 20% at OHP and CAV, and for 14% at SME.

Regarding wind speed, SME presents the highest mean (6.7 m s^{-1}), followed by CAV (3.8 m s^{-1}) and OHP (3.7 m s^{-1}). ERSA is the site with the lowest mean wind speed (2.4 m s^{-1}). At CAV, OHP and ERSA, wind speeds are mostly comprised between 2 and 6 m s^{-1} ("medium breeze"

Table 3
Definition of wind classes according to wind speed ($m.s^{-1}$) inspired by the Beaufort scale.

Wind class	Wind speed ($m.s^{-1}$)
Calm – Light breeze	≤2
Medium breeze	>2 to 4
High breeze	>4 to 6
Medium wind	>6 to 10
Strong wind	>10 to 17
Very strong wind	>17

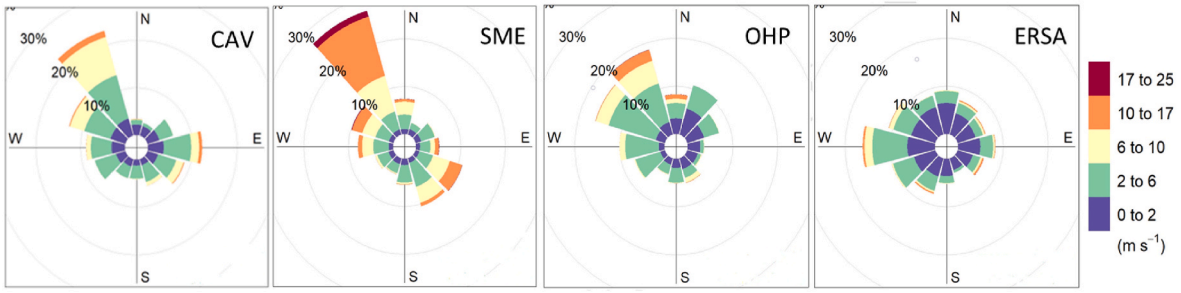

Fig. 3. Wind roses at the four sites on the 1 July 2016–31 January 2018 period, extracted from the WRF model data forced by ECMWF wind fields (see text). The wind speed scale is given accordingly to the wind classes defined in Table 3.

and "high breeze" classes), while at SME, the "medium wind" class (>6–10 m s^{-1}) is as frequent (33%) as the "medium breeze" and "hight breeze" ones merged together. SME is also characterized by a higher occurrence of "strong winds" (>10–17 m s^{-1}, 23%) as well as some events of "very strong winds" (>10 m s^{-1}). Conversely, ERSA presents a higher frequency of the "calm – light breeze" class (≤2 m s^{-1}) than the three other sites.

There are other noticeable differences between the four sites. In the NE sector, the Mistral "medium wind class" is relatively well represented at CAV and SME. However, at CAV, Mistral is characterised by wind speeds lower than at SME (Fig. 3). Indeed, the reliefs surrounding the NW sector of the city slow down the air masses advected on this latter (Puygrenier et al., 2005). Furthermore, Lemonsu et al. (2006) noticed that the Mistral is slowed down over Marseille because the roughness of the urban surface is higher than the rural surroundings one. At CAV, the Mistral can thus also partly enter into the high breeze class (Table 3, Fig. 3). As an example, Lemonsu et al. (2006) measured wind speed between 5.5 m s^{-1} and 7 m s^{-1} during a Mistral episode in Marseille. Moreover, SME is located on the city coast, where winds are generally more intense than inland (Bordreuil et al., 1973; Guenard et al., 2005). Wind speeds higher than 15 m.s^{-1} occur at SME during winter, entering into the strong wind and very strong wind classes (Table 3, Fig. 3). While at OHP, the main wind pattern differences with the CAV and SME sites are within the SE sector that is less represented, and within the NE sector that is more occurrent. At ERSA, the W direction is the most occurrent, conversely to the other sites.

Furthermore, the southern part of the SUD-PACA region is influenced by land/sea breezes due to its proximity to the Mediterranean Sea (mostly during summertime). Previous studies in the Aix-Marseille area have shown that sea breezes can typically penetrate over 100–150 km inland (Drobinski et al., 2006, 2018). The development of the land/sea breezes process occurs under cloud-free conditions and originates from the air temperature difference between the land and the sea. During daytime, this thermal contrast generates a local-scale pressure gradient from the sea to land, and thus a shallow layer of marine air moves inland, forming a sea breeze (Miller et al., 2003). The gradient can be reversed at night, and a land breeze blows toward the sea. In Marseille, this process generates southerly and south-westerly winds during sea breeze situations and north-easterly winds during land breeze ones. In the early 2000s, the ESCOMPTE campaigns allowed a better understanding of these specific winds in this area, and provided the following information: 1/sea breeze generally blows between 2 and 4 m s^{-1} (Kalthoff et al., 2005; Puygrenier et al., 2005) - and is therefore included in the "medium breeze" class -; and 2/land breeze is generally less intense than sea breeze (Bastin et al., 2005) – and is therefore rather included in the calm-light breeze class. These conclusions are in agreement with the analysis of our dataset: in Summer, the "medium breeze" class in the SW sector at CAV represents 24% of winds during daytime but only 14% at nighttime; the same wind class in the NE sector is less frequent than in the SW sector, but as expected more frequent at nighttime (5%) than during daytime (3%). Similar results are obtained for the SME site. Regarding the light breeze class, the SW sector represents, at CAV and SME respectively, 24% and 15% of the data during daytime vs 14% and 10% during nighttime, while the NE sector accounts for 3% at both sites during daytime vs 5% and 6% during nighttime.

To assess the spatial representativity of each site, mean airmass backtrajectories were computed for each season between 1 July 2016 and 23 February 2018 using the NOAA HYSPLIT model (Stein et al., 2015; Rolph et al., 2017) forced by Global Data Assimilation System (GDAS) meteorological fields reanalysis, at a 0.5° resolution and on a period of 72 h backward with a time step of 6 h. The altitude above ground level for computing the trajectories is the sampling height of each site given in Table 1 (we used the CAV sampling height for both CAV and SME sites). These backtrajectories were clustered in 8 wind direction cones of 45° each to calculate the contribution of short to long-range air masses originating from each cone to each site. The clustering method is implemented within HYSPLIT and is explained online (https://www.ready.noaa.gov/documents/Tutorial/html/traj_cluseqn.html). It consists in calculating the variations of the total spatial variance between the different clusters and the spatial variance between each cluster component. Trajectories are combined into the same cluster until the total variance between the individual trajectories begins to increase. Differences among individual elements of each cluster are minimized while the differences among the members of the different clusters are maximized. The number of clusters can be chosen by the operator. More details can be found in Stunder (1996) and Draxler (1999). The mean trajectory and the relative contribution of the different clusters are shown for the 4 sites and per season in the Supplementary Material section (S1) and are used to support the analysis performed in Section 3.

3. Results and discussion

In the following, time is always given in Coordinated Universal Time (UTC) units. The comparison between the different stations was performed on the period during which the four stations delivered data almost all the time (1 July 2016 to 13 February 2018), called "the common period" here after; however, due to instrumental failures, there are only a few data at ERSA in winter 2017/2018 and no data in springtime at SME.

3.1. Growth rate and distribution of atmospheric CO_2 at the four sites

Fig. 4 shows the timeseries of hourly atmospheric CO_2 concentrations collected at the four sites for different periods, the longest being from 25 April 2013 to 5 February 2018. In this section, the 10 m AGL dataset is used for OHP. The observation period is not long enough to determine a trend. However, the two longer series show an annually average CO_2 increase of 2.2 ± 0.8 ppm/year over the 3 full years covered by the OHP dataset and 2.9 ± 0.2 ppm/year at ERSA over the same period. These values obtained at OHP and at ERSA are a bit lower and slightly higher respectively to the northern hemisphere mean growth rate observed over the same period at the Mauna Loa ESRL/

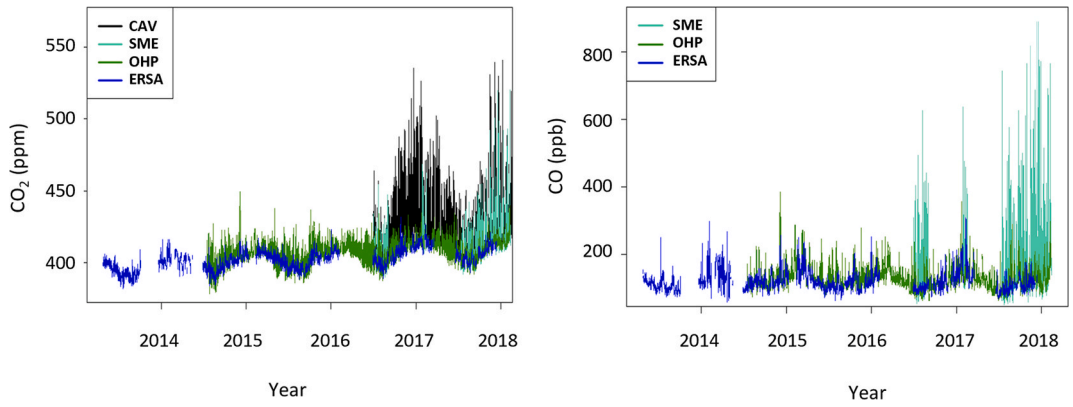

Fig. 4. Atmospheric CO_2 (left) and CO (right) concentration timeseries collected at the four observation sites between April 2013 and February 2018. The OHP dataset shown here was collected at 10 m AGL.

NOAA reference site (2.45 ± 0.55 ppm/yr, with an uncertainty of 0.11 ppm/yr); https://www.esrl.noaa.gov/gmd/ccgg/trends/gr.html). The OHP and ERSA datasets are influenced by different local, regional and remote emissions (see section 3.4.2) which can explain these differences. In the case of OHP, Lelandais et al. (2022) showed that about 16% of the data collected at this site are contaminated by local to remote sources, mostly traffic and residential heating. A deeper analysis of the annual CO_2 growth rate variability at OHP and its comparison with the one monitored at Mauna Loa can be found in Lelandais et al. (2022).

Table 4 gives some descriptive statistics of atmospheric CO_2 at each site. On the common period (1 July 2016–13 February 2018), CAV presents the highest CO_2 mean and variability (expressed as ±1 standard deviation of the mean) and median concentrations (423.9 ± 17.6 ppm and 419.6 ppm, respectively) and the largest variability. SME shows the second highest CO_2 mean concentration – which is more than 20 ppm lower than at CAV - and variability (411.7 ± 13.8 ppm). The median concentration is slightly lower that at OHP (0.3 ppm of difference only). The regional background stations (OHP and ERSA) are characterized by a lower CO_2 mean concentration (409.3 ppm and 406.3 ppm, resp.) and a weaker variability (6.9 ppm and 6.0 ppm, resp.), with ERSA showing the lowest values among the four sites. The CO_2 concentration range is also higher at both urban sites than at both background sites. Both urban sites are characterized by higher CO_2 third quartiles and interquartiles that at the background sites as they are closer to the places where urban emissions outcome form, especially CAV. The Yule-Kendall index (Table 4), which provides information on the skewness of the datasets, is positive at CAV (almost equals to 0.5) which is consistent with the influence of local urban sources that generate higher CO_2 concentrations at that station. At SME, OHP and ERSA, the Yule-Kendall index is slightly negative but most of all close to zero.

Atmospheric carbon monoxide (CO) is a tracer of combustion often used to better identify the impact of anthropogenic CO_2 sources on atmospheric CO_2 (e.g. Ammoura et al., 2016; Turnbull et al., 2015; Lopez et al., 2013). The CO timeseries show similar temporal features to the CO_2 ones, with frequent and rapid variations in Marseille. The urban timeseries are characterized by numerous concentration spikes with enhancements up to 750 ppb of CO at SME and up to 100 ppm of CO_2 at SME and CAV above the concentration levels measured at the OHP and ERSA background sites (Fig. 4). Unfortunately, CAV was not equipped with any CO instrumentation (Table 2). According to Table 2, on the period common to all sites, SME is characterized by the highest CO concentration mean and variability (161.5 ± 87.4 ppb), the highest median (136.8 ppb) and the highest CO maximum (885.3 ppb), which is explained by the proximity of this site to fresh urban combustion sources (traffic, heating). The interquartile is also the highest at SME as expected from this proximity, as is the Yule Kendall index (2.245) which shows the influence of high CO concentration values on the station dataset. OHP and ERSA show lower CO mean, median and variability, as well as lower minima, with the lowest values encountered at ERSA. The enrichment of the coastal site in CO as compared to both background

Table 4
Main statistics on the CO_2 and CO datasets (the OHP dataset is the 10 m AGL level one). The common period tested here is 1 July 2016 to 13 February 2018. The full period correspond to the period covered by the measurements at the given site according to Table 2. The data used for the calculation here are not detrended.

	CAV (common period)	SME (common period)	OHP (full period)	OHP (common period)	ERSA (full period)	ERSA (common period)
	CO_2 (ppm)					
Minimum	393.0	387.8	378.5	387.5	382.0	388.8
1st quartile	412.8	402.1	402.5	404.6	397.0	401.5
3rd quartile	430.7	417.7	411.9	414.0	406.3	410.9
Maximum	541.0	520.3	452.5	440.9	431.8	431.8
Mean	423.9	411.7	407.0	409.3	401.8	406.3
Standard deviation	17.6	13.8	7.4	6.9	6.7	6.0
Median	419.6	410.0	407.5	410.3	402.0	406.3
Interquartile	17.9	15.6	9.4	9.4	9.3	9.4
Yule Kendall Index	0.462	−0.021	−0.064	−0.213	−0.075	−0.022
	CO (ppb)					
Minimum	–	50.6	63.8	63.8	57.5	68.5
1st quartile	–	104.5	109.1	100.1	101.0	98.1
3rd quartile	–	190.2	141.1	138.6	130.2	129.6
Maximum	–	885.3	385.2	357.5	309.2	309.2
Mean	–	161.5	128.8	123.0	118.8	117.0
Standard deviation	–	87.4	30.3	29.9	26.1	29.4
Median	–	136.8	121.0	116.5	114.1	109.7
Interquartile	–	85.7	32	38.5	29.2	31.5
Yule Kendall Index	–	2.245	0.872	0.606	0.319	0.883

sites is also visible on the 3rd quartile which is at least 35% higher at SME than at OHP and at ERSA. These latters are both characterized by Yule-Kendall indexes lower than 1.

All of the four sites are characterized by a well-marked CO_2 seasonality and a diurnal variability, as well as a variability at the synoptic scale that are analyzed in the following sections. The stations also display significant differences, as the sites located in Marseille city show higher CO_2 and CO concentrations and a larger variability than the ERSA and OHP stations. The presence of short CO spikes concomitant with CO_2 at SME is typical of the contribution of local anthropogenic emissions (e.g. Lopez et al., 2013). These spikes are much less often observed at both regional background sites. The higher CO_2 concentrations observed at SME and CAV sites are mostly linked to their proximity to urban anthropogenic sources (Gratani et Varone, 2004, Lopez et al., 2013; Staufer et al., 2016; Xueref-Remy et al., 2018). However, an average difference of 12.2 ppm can be observed between the CO_2 means of these two stations, both located in Marseille city. CAV presents higher CO_2 concentrations than SME explained by its location in the city center, whereas SME is situated on the coast of Marseille, facing the sea (SW and NW sectors). Wind regimes are known to have an impact on atmospheric CO_2 variability (e.g. Xueref-Remy et al., 2018), which is evaluated for the present study in Section 3.4. Finally, the mean CO_2 and CO concentrations are higher and more variable at OHP than at ERSA. While ERSA is mostly surrounded by the Mediterranean Sea, OHP is a continental site relatively far from large cities, in a region that is highly urbanized and industrialized and that contributes to increasing the regional background concentration (Lelandais et al., 2022), and also in the vicinity of small conurbations. The influence of local, regional and remote sources on the different sites is analyzed further in Section 3.4.

3.2. Diurnal variations

Atmospheric CO_2 most often follows a diurnal cycle, mainly on continental sites, which features are controlled by several factors, such as ABLH dynamics, the proximity of the observation site to anthropogenic emissions and their variability, its proximity to continental vegetation and the variability of their fluxes, its proximity to the sea, altitude of the site, altitude of the sampling height, season, climate and meteorological variations (e.g. Nasrallah et al., 2003; Gratani and Varone, 2005; Garcia et al., 2010; Rice and Bostrom, 2011; Fang et al., 2014; Huang et al., 2014; Xueref-Remy et al., 2018).

Fig. 5a represents the CO_2 mean diurnal cycle at each site calculated from CO_2 hourly averages (using the 10m level for OHP) on the common period (1 July 2016–13 February 2018). Before averaging, corrections were applied on the datasets, consisting of subtracting the annual rate of increase observed at each site and interpolated by month. The datasets have also been deseasonalized by applying the following method, citing Xueref-Remy et al. (2018): "(1) computing the annual mean of the dataset; (2) computing the monthly seasonal index for each month by calculating the ratio between the monthly mean and the annual mean of the dataset; (3) interpolating the monthly seasonal indexes at an hourly scale over the full period of study; and (4) dividing the CO_2 hourly dataset by the hourly seasonal index". A mean daily gradient of several ppm between the sites that increases with their exposure to anthropogenic emissions can be observed, reaching about 25 ppm between ERSA and CAV. The latter shows the highest diurnal amplitude (18.8 ppm), followed by SME (14.5 ppm), OHP (5.3 ppm). Then ERSA has the lowest diurnal amplitude (0.5 ppm): the amplitude of the diurnal cycle also increases with the proximity of the site to urban CO_2 emissions. Fig. 5e, f, 5g and 5h show the 1-σ variability associated with the hourly means of the CO_2 diurnal cycle for CAV, SME, OHP and ERSA, respectively. This variability also increases with the proximity of the site to anthropogenic sources, ranging within ±4 ppm at any hour of the day at ERSA and within ±7 ppm at OHP, from ±6 ppm to ±15.5 ppm (07h00) at SME and from ±7 ppm (14h00) to ±19 ppm (06h00 and 07h00) at CAV. This can be explained by the large variability of anthropogenic sources and lower atmospheric mixing of "fresh" sources in the urban environment vs background ones that are mostly exposed to well-mixed air masses. Similar observations regarding the gradient between the sites, the amplitude and the variability of the CO_2 diurnal cycle were found in other urban studies, e.g. within the CO_2-MEGAPARIS project on Paris megacity (Xueref-Remy et al., 2018) and within the INFLUX project on Indianapolis (Turnbull et al., 2015).

The CO daily mean and diurnal cycle amplitude, also computed with hourly averages (Fig. 5b), show identical features to the CO_2 ones. SME is characterized by a CO daily mean (diurnal amplitude) of about 170 ppb (63.0 ppb), against 123.6 ppb (2.2 ppb) for OHP, and 118.5 ppb (0.4 ppb) for ERSA. Compared to background concentration levels, the urban atmosphere is thus enriched in CO and CO is also much more variable. As mentioned earlier, CO has not been monitored at CAV. However, NOx has been recorded (Fig. 5c) and can be used as a tracer of CO_2 anthropogenic emissions, mainly from traffic (e.g. Lopez et al., 2013; Ammoura et al., 2014; Ammoura et al., 2016). The NOx amplitude at CAV is about 40 $\mu g/m^3$, which corresponds to a 4 times increase of the lowest NOx concentration encountered at the station. Thus at the urban sites, CO_2, CO and NOx show a relatively large variability in comparison to the background stations, with a temporal variability that is analyzed next to infer the nature of the anthropogenic sources contributing to the urban stations.

A daily maximum of CO_2 is clearly observed at CAV and SME (432.1 ppm and 419.0 ppm, respectively) in the morning between 06h00 and 07h00. Simultaneously, the CO diurnal cycle gets maximum at SME (198.7 ppb) and the NO_X one at CAV (49.1 $\mu g/m^3$). These peaks are concomitant to the morning traffic peak in Marseille that goes from 05h00 to 06h00 to 06h00-07h00 (https://www.tomtom.com/en_gb/traffic-index/marseille-traffic/). Therefore, the traffic sector seems to control the CO_2 morning peak at both urban sites. At ERSA, the diurnal cycle is almost flat (mean of 403.9 ppm) and gets its maximum at 06h00 (404.2 ppm). At OHP (see Fig. 6, 10 m AGL level), there is a maximum of CO_2 at night at 04h00 (408.7 ppm) and a second maximum in the morning at 07h00-08h00 around 408.2 ppm. In the following hours, a decrease in the mean CO_2 concentration is observed at all sites to reach a minimum at 11h00 at ERSA (403.7 ppm), at 14h00 at OHP (403.4 ppm, respectively), at 15h00 at SME (404.5 ppm) and at 14h00 at CAV (413.3 ppm). At CAV and SME, this decrease is associated with a minimum in NO_X and CO. Finally, the concentrations increase again at the end of day.

The diurnal cycles of CO and NOx follow the same pattern at the urban sites with a second peak at the end of the day. At SME, a second maximum (~412 ppm) can also be observed on the CO_2 diurnal cycle around 21h00, which is concomitant with peaks on the CO diurnal cycle (~196 ppb, 20h00-21h00). At CAV, the NOx diurnal cycle also shows a second maximum but earlier (18h00-19h00) peaking at 40 ppb. The NOx maximum occurs during the evening traffic peak in Marseille, which extends on average from 16h00–19h00 (https://www.tomtom.com/en_gb/traffic-index/marseille-traffic/). The CO_2 and CO maxima at SME occur after the traffic peak. Thus, while the presence of CO indicates the contribution of an anthropogenic source, this latter cannot be traffic. According to the ATMOSUD CO_2 emissions inventory for Marseille city, road traffic and domestic heating are the dominant CO_2 emission sectors for this area - respectively 41.4% (mostly based on the combustion of oil for 38.5%, bioenergies for 3.7% and gas for 0.05%) and 32% (mostly based on the combustion of natural gas for 24.1%, petroleum fuels for 5.7% and wood burning for 1.4%) (https://cigale.atmosud.org/). These peaks are rather due to domestic heating, which is stronger when people are at home, in the evening and in the early nighttime. Domestic heating is known to occur in Marseille in the evening and at night in Marseille from observations of particulate matter and black carbon (https://www.atmosud.org/sites/paca/files/atoms/files/191205_atmosud_rapport_bc_2018.pdf). A deeper insight into the role of the heating sector vs traffic on atmospheric CO_2 in Marseille is assessed in the next section by analyzing the seasonal variability of the diurnal cycle of CO_2, CO and NOx.

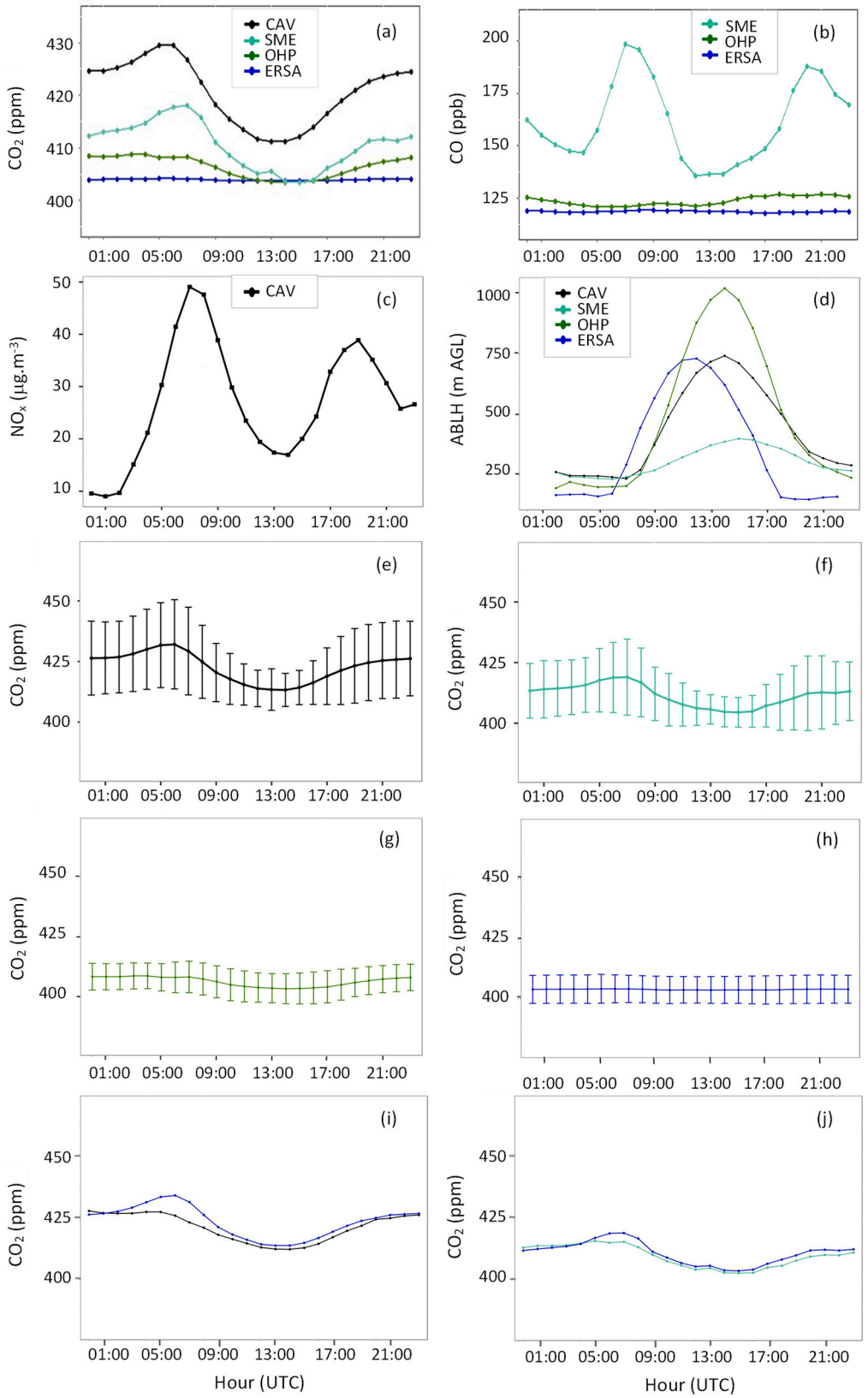

Fig. 5. (a) Mean diurnal cycles of CO_2 at the four observation sites on the common observation period (01072016–13022018); (b) Mean diurnal cycles of CO at all observing sites but CAV; (c) Mean diurnal cycle of NO_X at CAV; (d) Mean diurnal cycles of the ABLH at the four observation sites; (e) 1-σ standard deviation of CO_2 hourly means at CAV; (f) 1-σ standard deviation of CO_2 hourly means at SME; (g) 1-σ standard deviation of CO_2 hourly means at OHP; (h) 1-σ standard deviation of CO_2 hourly means at ERSA; (i) Weekday (blue) and weekend (black) CO_2 diurnal cycles at CAV; (j) Weekday (blue) and weekend (cyan) CO_2 diurnal cycles at SME. (For interpretation of the references to colour in this figure legend, the reader is referred to the Web version of this article.)

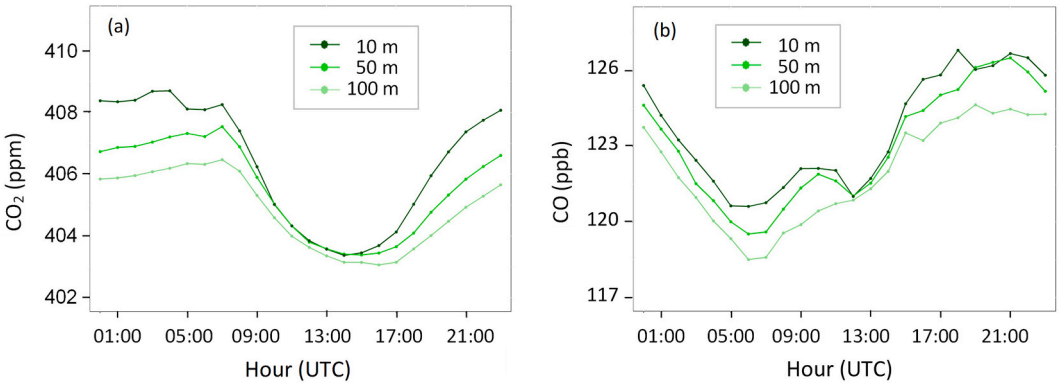

Fig. 6. Mean diurnal cycles of CO_2 (a) and CO (b) collected at 10, 50 and 100 m AGL at OHP.

The ABLH modulates atmospheric CO_2 on the course of its own diurnal cycle (e.g. Xueref-Remy et al., 2018). Fig. 5d shows that the ABLH varies daily as expected (e.g. Pal et al., 2012) with site-specific patterns. At night, it stands between 150 and 250 m AGL, depending on the station. It increases in the morning (07h00 – 08h00), more or less intensively from one site to another, to reach its maximum in the afternoon. At the continental site OHP, the ABLH maximum reaches 1019 m AGL, while it peaks at 400 m AGL at SME, which is influenced by both continental and marine air mass dynamics. On the CAV and ERSA sites, the ABL culminates in a middle range compared to OHP and SME, at 740 m AGL and 730 m AGL, respectively. At all the sites but ERSA, the maximum of the ABLH is correlated with the minimum of the CO_2 diurnal cycle (at ERSA, the CO_2 diurnal variability is so low that there is no maximum peak). At CAV and SME, the CO_2 maxima observed in the morning (Fig. 5a) are not correlated to a decrease in the ABLH, and thus are not strongly driven by ABL dynamics. The simultaneous increase of CO and NOx (Fig. 5b and c) together with CO_2 proves that combustion sources are the main controller factor of the diurnal cycle peak at the two urban sites. As mentioned above, these maxima can be mostly explained by the morning traffic intensification during rush hours in Marseille, in a steady ABL (Fig. 5d). Later during the day, atmospheric CO_2 decreases together with CO and NOx, reaching their minima in the early afternoon. This decrease occurs in the afternoon when the ABLH is increasing at both sites. The elevation of the ABL creates a vertical dilution of CO_2 sources, explaining partly why the CO_2 concentration is dropping. The second cause of this decrease is that urban CO_2 emissions are at their minimum in the afternoon (lower traffic and lower heating, https://www.atmosud.org/sites/paca/files/atoms/files/191205_atmosud_rapport_bc_2018.pdf). At the end of the day, CO_2 increases due to the ABLH decrease, and as mentioned above, to traffic and heating emissions increase as indicated by the increase of NO_X and CO in the evening and early night.

At ERSA, the hourly mean CO_2 concentration is almost stable during the course of the day, mostly due to the proximity of this site to the sea, which surrounds most of the site. There is no CO_2 anthropogenic source near this station, conversely to the case of the CAV and SME sites, which proximity to urban CO_2 sources noticeably controls the shape of the CO_2 diurnal cycle. Despite the thickening of the ABL indicated by the WRF model, the ABLH does not seem to play an important role on the CO_2 diurnal variability at ERSA. Indeed, the ABLH diurnal cycle at this site is not the one expected for a site like ERSA, which is situated near the sea. It should therefore show similar features to that of SME, with a lower amplitude because the ABL thickness is generally weaker during daytime in coastal areas than inland as the marine ABL influences it (e.g. Brahmanandam et al., 2020; Lemonsu et al., 2006). The ABLH values are indeed extracted for ERSA from a 2×2 km^2 cell of our WRF modeling framework that is centred inland, and thus not much representative of the coastal area. However, the small variations in CO_2 observed at ERSA make it a good site for background atmospheric concentrations in a marine environment. At OHP, the ABLH diurnal cycle variation is opposite to the one of CO_2: CO_2 is maximum when ABLH is minimum and vice-versa. ABL dynamics partly control CO_2, together with the activity of vegetation i.e. photosynthesis during daytime that lowers atmospheric CO_2, and respiration during nighttime that increases atmospheric CO_2 at this background forested site (e.g. Xueref-Remy et al., 2018; Schmidt et al., 2011). The influence of anthropogenic emissions is not visible at the diurnal scale at OHP, as shown by the lower levels and low amplitude of the CO diurnal cycle at this site in comparison with what is observed at CAV site.

Atmospheric CO_2 can also be impacted by the variability of urban activities in function of the days of a week and especially of traffic, which is higher during weekdays than during weekends at the moment of morning rush hours (4–5 times more congested) and evening ones (1.5 to twice more congested) (https://www.tomtom.com/en_gb/traffic-index/marseille-traffic/). Fig. 5i and j show the CO_2 diurnal cycles for weekdays and weekends at CAV and SME, respectively. At both stations, a concentration maximum clearly appears on the CO_2 diurnal cycle at the time of the morning traffic peak during weekdays compared to weekends when no such maximum is observed (+8.5 ppm at 06h00 for CAV and +4 ppm at 06h00 and 06h00 for SME): this is consistent with the large increase of traffic during weekdays vs weekends during morning rush hours. Conversely, the increase of traffic observed in the evening during weekdays compared to weekends does not noticeably modify the shape of the CO_2 diurnal cycle, possibly because the traffic peak increase during weekdays vs weekends is much lower in the evening than in the morning, as mentioned above.

The sampling height also controls the shape of the atmospheric CO_2 diurnal cycle (e.g. Vermeulen et al., 2011; Schmidt et al., 2014; Xueref-Remy et al., 2018; Conil et al., 2019). At OHP, CO_2 and CO measurements are carried out at three different heights (10, 50 and 100 m AGL). A recent study deeply analyzes the atmospheric CO_2 variability at this site (Lelandais et al., 2022). Fig. 6 shows the mean diurnal cycles of CO_2 (Fig. 6a) and CO (Fig. 6b) at OHP for each sampling level. At 10 m, the maximum of CO_2 is observed at 04h00, followed by a second maximum at 07h00, which is present at the three sampling levels. Thereafter, the three cycles follow the same scheme. However, the amplitude of the CO_2 diurnal cycle decreases with the inlet height due to atmospheric mixing, as already observed at other ICOS sites equipped with tall towers (e.g. Vermeulen et al., 2011; Schmidt et al., 2014; Conil et al., 2019). It extends to 5.3 ppm, 4.1 ppm and 3.4 ppm at 10 m, 50 m and 100 m AGL respectively. Furthermore, the maximum of CO_2 is higher at 10m AGL than at 50 m AGL, because at 10 m AGL the air inlet is closer to natural and anthropogenic local fluxes and the maximum occurs during the night, when the atmosphere is stable and these fluxes do not get well mixed, staying close to the ground level. The 10 m level and the 50 m AGL show almost the same minimum concentrations during daytime, probably because of the vertical atmospheric mixing of local sources. At 100 m AGL, the maximum and the minimum of the CO_2 diurnal cycle are

both lower than at 10 m and 50 m AGL, showing that this level of the OHP tower is less controlled by local fluxes, and that it rather samples more mixed air masses, being more representative of a larger area than the two lower levels. The OHP 100 m AGL timeseries can thus be considered as a better regional background signal than the 10 m and the 50 m AGL ones (see more details in Lelandais et al., 2022).

As for CO_2, the maximum of the CO diurnal cycle decreases with the height of the sampling level, but also the daily mean CO concentration - although the differences between the levels are tiny (≤3 ppb). The amplitude of this cycle is very low for each level (≤7 ppb), and the CO minima are observed at 06h00 for all levels. The 10 m and 50 m AGL levels show an intermediate peak between 08h00 and 11h00 and the maximum of CO between 18h00 and 21h00. These peaks are likely related to anthropogenic combustion sources, mostly traffic and heating from nearby urbanized areas (e.g. Saint-Michel-l'Observatoire, Manosque). The smoother diurnal cycle of CO at 100 m AGL level confirms that this level is rather under the influence of atmospheric dynamics and long-range transport rather than local fluxes. A deeper study on the representativity of OHP and on the impact of anthropogenic sources at this site can be found in Lelandais et al. (2022), which estimate this impact of the order of 20%, with about 80% of the data representative of regional background CO_2 concentrations.

3.3. -Seasonal variations

The CO_2 seasonal cycles are presented in Fig. 7a for the four observation sites. The data used to calculate these cycles are based on the hourly dataset detrended from the annual increase, then averaged by month. Let us recall that due to several instrumental issues, there is no data at SME for the months of March to July. Several factors are known to control the atmospheric CO_2 seasonal cycle (e.g. Xueref-Remy et al., 2018), which is mostly variable over the continents: (1) the proximity of the site to vegetation fluxes and the seasonal activity of the biosphere, (2) the proximity of the site and the variability of anthropogenic emissions; (3) the seasonal cycle of the ABLH at the site; and (4) meteorological and especially wind variations. The impact of these latter is analyzed in Section 3.4.

Vegetation activity modulates atmospheric CO_2 at the seasonal scale

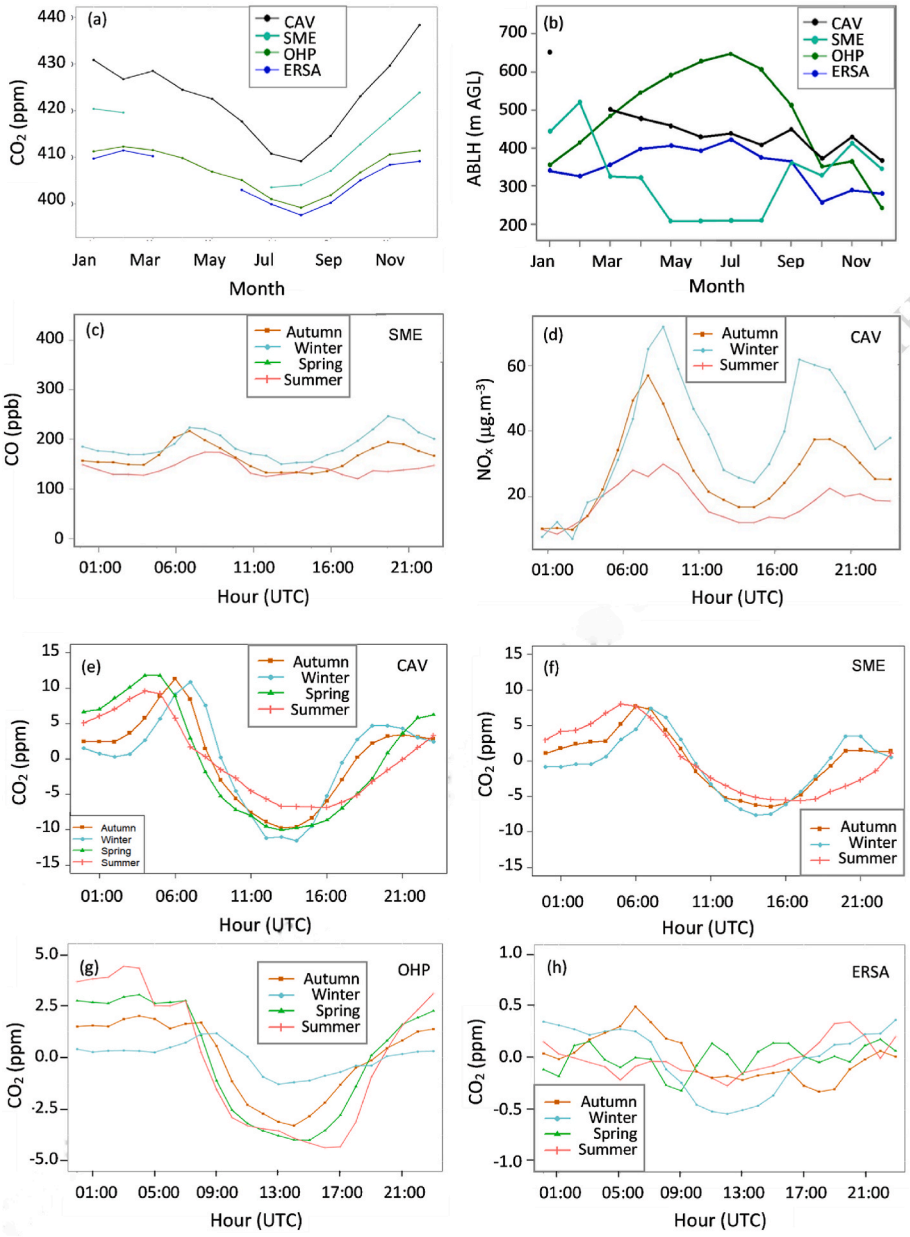

Fig. 7. (a) Seasonal cycle of CO_2 at the 4 observation sites (monthly means); (b) Seasonal cycle of the ABL height at the 4 observation sites (monthly means from Jan 2016 to Fev 2018); (c) to (h) Diurnal cycles of CO_2 calculated by season at CAV, SME, OHP and ERSA, respectively (hourly means). To produce (a) to (h), the data were corrected from the annual trend at each site. For (c) to (h), the data were also seasonally normalized before the calculation of the monthly means, as explained in the text. The lack of data at SME from March to June is due to instrumental issues.

through both photosynthesis and respiration processes (Nasrallah et al., 2003; Huang et al., 2015; Xueref-Remy et al., 2018). In winter, photosynthesis is much weaker and atmospheric CO_2 is therefore much less absorbed by vegetation: the respiration process is dominant and gets the atmosphere enriched in CO_2. In Spring, vegetation grows and uptakes CO_2 from the atmosphere until Summer. Thereafter, atmospheric CO_2 concentration increases again, in parallel with the photosynthetic activity's slowdown until the end of the year, when a new seasonal cycle starts. Vegetation fluxes usually strongly impact atmospheric CO_2 on background forested sites such as OHP, as discussed a bit further and deeply analyzed in Lelandais et al. (2022).

The ABLH also varies at the seasonal scale, usually reaching its minimum in Winter and its maximum in Summer (e.g. Stull, 1988). This behavior tends to increase atmospheric CO_2 in Winter and to decrease it in Summer, and partially controls atmospheric CO_2 on the four sites (Fig. 7b).

Due to its higher proximity to urban emissions, CAV always displays the highest monthly CO_2 averages compared to SME, then OHP and eventually ERSA. The seasonal variability of atmospheric CO_2 shows some similar features at the four sites: the monthly CO_2 mean concentration decreases from the beginning of the year until Summer and it increases in the second half of the year. The maximum of the CO_2 seasonal cycle is observed in December in Marseille city (438.4 ppm at CAV and 423.9 ppm at SME), and in February at OHP and ERSA (407.3 ppm and 405.5 ppm, respectively). At CAV, a relative decrease of CO_2 is visible in February, due to specific synoptic meteorological conditions at this period: the wind speed seasonal cycle presents a rise in February in Marseille city, hence a diminution of the monthly mean CO_2 through more intense dispersion. The amplitude of the seasonal cycle is higher at the urban sites (29.2 ppm at CAV and 20.3 ppm at SME) than at the background sites (13.1 ppm at OHP and 13.9 ppm at ERSA). Furthermore, the 1-σ variability of the monthly means is (1) relatively low at both background sites (4.6 ppm at OHP and 5.0 ppm at ERSA); and (2) it is much larger at the urban sites (from 8 ppm in July to 17 ppm in December at SME and from 9.5 ppm in August to 21.5 ppm in January) likely from the impact of anthropogenic emissions as indicated by the larger CO_2 variability in the cold months. Thus, the annual mean, the monthly means, the amplitude and the variability of the seasonal cycles are controlled partly by their proximity to biospheric fluxes and to urban emissions. Such seasonal features have also been observed in previous urban studies (e.g. Turnbull et al., 2015; Xueref-Remy et al., 2018). The impact of the ABLH seasonal dynamics is addressed further below.

In order to better constrain the role played by natural fluxes and anthropogenic emissions on atmospheric CO_2 seasonal variability, the mean diurnal cycles of CO_2 are shown by season (Fig. 7e–h), calculated from the datasets detrended from the annual increase observed at each site and then seasonally normalized (cf section 3.2). The CO and NOx diurnal cycles are also plotted by season.

In Marseille, both at CAV and SME, the CO_2 diurnal amplitude is greater in Winter (22.5 ppm and 15.0 ppm respectively) than in Summer (16.4 ppm and 13.6 ppm respectively). On top of the impact of the ABLH seasonal variability discussed above, this is an indicator of the contribution of anthropogenic emissions on these two urban sites. The heating sector primarily drives the CO_2 seasonality because of the drop of the air temperature during that season. According to the ATMOSUD inventory, CO_2 emissions from this sector in Marseille are ~4 times larger in Winter than in Summer, although the activity estimates are inaccurate (S. Oppo, ATMOSUD, personal communication). Conversely, at OHP (Fig. 7g), the amplitude is the highest in Summer (9.8 ppm) and the lowest in Winter (2.7 ppm), which is an indicator of the contribution of continental biospheric fluxes at OHP as vegetation is active mostly in Spring and Summer, as expected for this forested background site (Lelandais et al., 2022). Finally, at ERSA, the amplitude is very low, generally less than 1 ppm (Fig. 7h), which indicates that there is no significant contribution of anthropogenic emissions nor of continental biospheric fluxes on this background station located in a marine environment.

At CAV and SME, the impact of anthropogenic activities on the CO_2 and CO diurnal cycles is primarily visible in Autumn and Winter, while being observable in all seasons on the NOx diurnal cycle. This is mainly visible through morning and evening/early night peaks during traffic rush hours and domestic heating (see former section), which amplitude strongly depends on the season, as does the mean diurnal CO_2 concentration. In the morning, in Autumn and Winter, CO_2 peaks together with CO and NOx during rush hours, which indicates that these peaks are controlled by traffic. In Spring and Summer, the morning traffic peaks are less pronounced but still visible on NOx, although not visible on CO and CO_2. In the evening, in Autumn and Winter, CO_2 and CO peaks during rush hours, thereafter both continue to increase which testifies to the impact of the heating sector in the late night in the cold months. These late peaks are not more visible in the warmer seasons, either on CO_2 or on CO. The amplitude of the diurnal cycles is quite similar for all seasons, indicating that vegetation/CO_2 biospheric fluxes have a poor influence on the CAV and SME sites. The CO_2 fluxes exchanged by the atmosphere and the sea are much lower than the ones between the continental biosphere and the atmosphere (Friedlingstein et al., 2020; Wimart-Rousseau et al., 2020): their impact is thus even more negligible on these stations. Finally, let us recall that the ABLH is lower in the cold seasons than in the warm ones (cf Fig. 7b), and thus it tends to increase the daily mean atmospheric concentrations through the accumulation of anthropogenic emissions in a shallower atmospheric layer in Autumn and Winter.

At OHP, the larger amplitude of the diurnal cycle during Summer is for the main part the result of the activity of vegetation, which is absorbing CO_2 during daytime through the photosynthesis process, and is rejecting CO_2 during nighttime when it respires; the ABL diurnal and seasonal variability, as mentioned earlier, is the other controlling factor of atmospheric CO_2 at OHP. The tiny peak observed at 10 m AGL at OHP in Figs. 6a and 7g, around 03h00-04h00, is visible in all seasons except in the winter. Such a peak is not much apparent on the CO diurnal cycle (Fig. 6b), which supports an influence of vegetation fluxes rather than combustion processes on this peak Indeed, during the night in the warm months of the year, plants emit CO_2 by respiring, while in Winter when vegetation is dormant and exchanges much lower fluxes with the atmosphere (Vintejoux et Dereuddre, 1981; Nasrallah et al., 2003; Huang et al., 2015; Xueref-Remy et al., 2018). The CO_2 peak at 03h00-04h00 can thus be explained by the vegetation respiration process emitting CO_2 which accumulates close to the ground level in a steady nighttime ABL. This also explains the vertical gradient of CO_2 observed at OHP at night between 10 m and 100 m AGL (Fig. 6a). This gradient shows a decoupling between the highest sampling level and CO_2 surface fluxes at night (Schmidt et al., 2014; Xueref-Remy et al., 2018). After 04h00 at OHP, the CO_2 concentration decreases thanks to the photosynthetic activity of the surrounding vegetation and atmospheric mixing, with lower vertical gradients during daytime that nighttime. This shows that atmospheric CO_2 is mostly driven by biospheric fluxes and boundary layer dynamics at OHP, as deeply studied in Lelandais et al. (2022).

At ERSA, the features of the CO_2 diurnal cycle per season are quite similar for all seasons and there is no evidence of an impact of biospheric fluxes nor of anthropogenic emissions on the ERSA CO_2 seasonal cycle. There is only a small variability per hour contained within 1 ppm which depends on the season and that could be due to the variability of synoptic conditions and boundary layer dynamics. The impact of wind patterns is further analyzed in the next section.

Similar observations of seasonal gradients between urban and background sites of several ppm were found in previous urban CO_2 studies, depending on the environment, meteorology, atmospheric dynamics and sampling height at the observing stations (e.g. Turnbull et al., 2015; Xueref-Remy et al., 2018). A comparison can be made for example, with the Paris megacity study in which Xueref-Remy et al. (2018) assessed the impact of the different factors controlling atmospheric CO_2 in urban, peri-urban and background sites: they reported a larger mean seasonal cycle in densely urbanized sites at 5 m AGL than in

rural background ones at 50 m AGL (+15–20 ppm), a result that is of the same order of magnitude in the present Aix-Marseille study.

3.4. Influence of wind regimes

Together with ABLH dynamics as well as anthropogenic and natural fluxes, local and regional wind regimes also control the variability of urban CO_2 concentrations; furthermore, according to the wind regime, air masses have different origins which possibly leads to different CO_2 background levels upwind of the city (e.g. Xueref-Remy et al., 2018). Wind regimes vary from the hour for breezes to several days for synoptic air mass movements and by season, and thus play a role in the variability of CO_2 at these different temporal scales.

3.4.1. CO_2 vs wind speed

Wind speed has already been demonstrated to be a key parameter in modulating atmospheric CO_2. In several previous urban studies, a dome of CO_2 reaching several tens of ppm was observed over the city at low wind speeds (<3 m s^{-1}) in comparison to rural background concentrations from the accumulation of local anthropogenic emissions, for example in Phoenix (Idso et al., 2002) and in the Paris megacity (Xueref-Remy et al., 2018). For mid-wind speeds (3–10 m s^{-1}), advection transforms this dome into an urban plume of a few ppm to a few tens of ppm over background concentrations that is transported downwind of the city, as seen in Indianapolis (Turnbull et al., 2015), Los Angeles (Verhulst et al., 2017) and Paris (Xueref-Remy et al., 2018). The CO_2 urban plume was detected downwind of the city center in peri-urban sites located a few km to a few tens kilometres away from urban centers, but not on regional background sites (~100 km away) as the plume was dispersed before (Turnbull et al., 2015; Xueref-Remy et al., 2018). However, the recent study of Lelandais et al. (2022) shows that the urban plume emitted by the Aix-Marseille megacity can be transported to the OHP site (located about 70 km further north) under sea breeze regime for wind speed ~3–5 m s^{-1}, which leads to an increase of the CO_2 concentration at this site of a few ppm (which cannot be considered as a background site in these situations, as explained in Lelandais et al., 2022). For large wind speeds (>10 m s^{-1}), in all urban studies the plume almost vanished through ventilation processes, but still, a remaining CO_2 gradient of a very few ppm was observed between the urban sites and the background ones (e.g. in Paris megacity, Xueref-Remy et al., 2018), which was explained by the higher proximity of the urban and peri-urban sites to anthropogenic emissions compared to background ones.

The quantification of the urban dome/plume depends on the background site location, which should be, when the best suited, located at the rural/peri-urban border upwind of the studied urban area in order to avoid the influence of CO_2 fluxes between the city and the background location, for example from the biosphere (e.g. Turnbull et al., 2018; Xueref-Remy et al., 2018). Furthermore, several background sites can be needed to cover the direction of the different dominant winds, as air-masses can be influenced by different remote fluxes before their arrival upwind of the studied city, depending on their trajectory, possibly leading to noticeable differences of several ppm in CO_2 background levels (e.g. Turnbull et al., 2018; Xueref-Remy et al., 2018; Karion et al., 2021). In this study, although we did not have the funding to install such dedicated urban background sites, our datasets allow us to infer the strength and behavior of the urban signal depending on wind speed relatively to regional continental and marine background concentrations at OHP and ERSA, respectively. This information is especially important to provide for designing efficient intensive campaigns dedicated to inferring CO_2 emission sources from any atmospheric CO_2 urban dome/plume with the use of isotopes (e.g. Lopez et al., 2013) or CO_2 co-emitted species such as Volatile Organic Compounds (e.g. Ammoura et al., 2016).

The CO_2 mean concentration for each wind class and each site is given in Table 5 (calculated from the detrended datasets, see previous section). At CAV and SME, the mean concentration decreases from 423.0 ppm to 415.6 ppm–402.7 ppm and 403.7 ppm respectively when wind speed increases from 0 to 2 m s^{-1} to >17 m s^{-1}, with the strongest CO_2 decrease for wind speed higher than 6 m s^{-1}. At OHP, the mean concentration for wind speeds <2 m s^{-1} (408.2 ppm) is lower of ~15 ppm and ~7 ppm than at CAV and SME, respectively, but it does not decrease much when wind speed increases and even increases for strong and very strong winds, converging towards the concentration observed at the urban sites and then reaching higher concentrations for the largest wind speeds. At ERSA for wind speeds lower than 6 m s^{-1}, the mean concentration is almost stable around 403 ppm, being 20 ppm and 12 ppm lower than the CAV and SME mean concentrations. For higher wind speeds, the CO_2 mean concentration increased at ERSA reaching similar concentrations than at CAV and even larger ones for the highest wind speed events. For all ranges of wind speed, there are differences in the mean concentrations between the stations that depend on wind speed and that is maximum for the lowest wind speeds at the urban sites while it is maximum for the highest wind speeds at the background sites. Note also that the mean concentrations at SME site are always significantly lower (several ppm) than the mean concentrations at CAV, except for the "Very strong wind" class, which is very close.

Fig. 8 shows the hourly mean concentrations of CO_2 corrected from the annual trend interpolated by month as in section 3.2 as a function of wind speed and coloured by wind direction, at the four sites (the CO_2 concentration scale is adapted for each site). At OHP and ERSA, overall the hourly CO_2 concentrations vary within a range of 35 ppm. At CAV and SME, for wind speeds <5 m s^{-1} at CAV and <10 m s^{-1} at SME, the hourly CO_2 concentrations display a much larger variability towards higher concentration levels that reach 540 ppm at CAV and 505 ppm at SME. These features are observed at CAV for all wind directions and can have an amplitude of almost 150 ppm, and at SME for the NE and E sectors mostly where it can reach an amplitude of 100 ppm. These high concentration levels and large variability at the urban sites can be attributed to CO_2 emissions within Marseille, which accumulate over the city under the shape of a dome of CO_2 at low wind speeds (<2 m s^{-1}) and of a plume at higher wind speeds. This large distribution of CO_2 concentration are the result of the superimposition of anthropogenic emissions and natural fluxes, which relative partitioning is unknown yet but is currently under assessment through both a modeling work and a ^{14}C/CO/CO_2 field campaign approach following the methodology of Lopez et al. (2013). Such behavior of urban CO_2 concentration vs wind speed is similar to the one observed in other cities and the order of magnitude is similar to the ones observed in the Paris urban center. For the highest wind speeds, the CO_2 concentrations tends toward an asymptotic value (cf Table 5). An exponentiel decrease of CO_2 concentration is observed while wind speed increases at CAV and SME, that is not observed on the two background sites. This behavior has also been observed in former urban studies (e.g. Xueref-Remy et al., 2018).

3.4.2. Local, regional and remote contributions to atmospheric CO_2 at the four sites

To better assess how wind regimes control the CO_2 variability, Fig. 9a to Fig. 9d show the hourly mean concentrations of CO_2 in function of wind speed and direction by bins of 2 m s^{-1} and 10° at the four sites (so-called « CO_2 roses »), the associated standard deviation

Table 5
Mean CO_2 concentration for the different wind classes and sites of this study (detrented datasets).

Site name	Wind class (m.s^{-1})				
	0 to 2	>2 to 6	>6 to 10	>10 to 17	>17
CAV (ppm)	423.0	421.1	411.6	408.1	402.7
SME (ppm)	415.6	414.7	408.9	405.1	403.7
OHP (ppm)	408.2	406.1	404.3	405.8	408.5
ERSA (ppm)	403.1	403.4	406.0	407.7	409.5

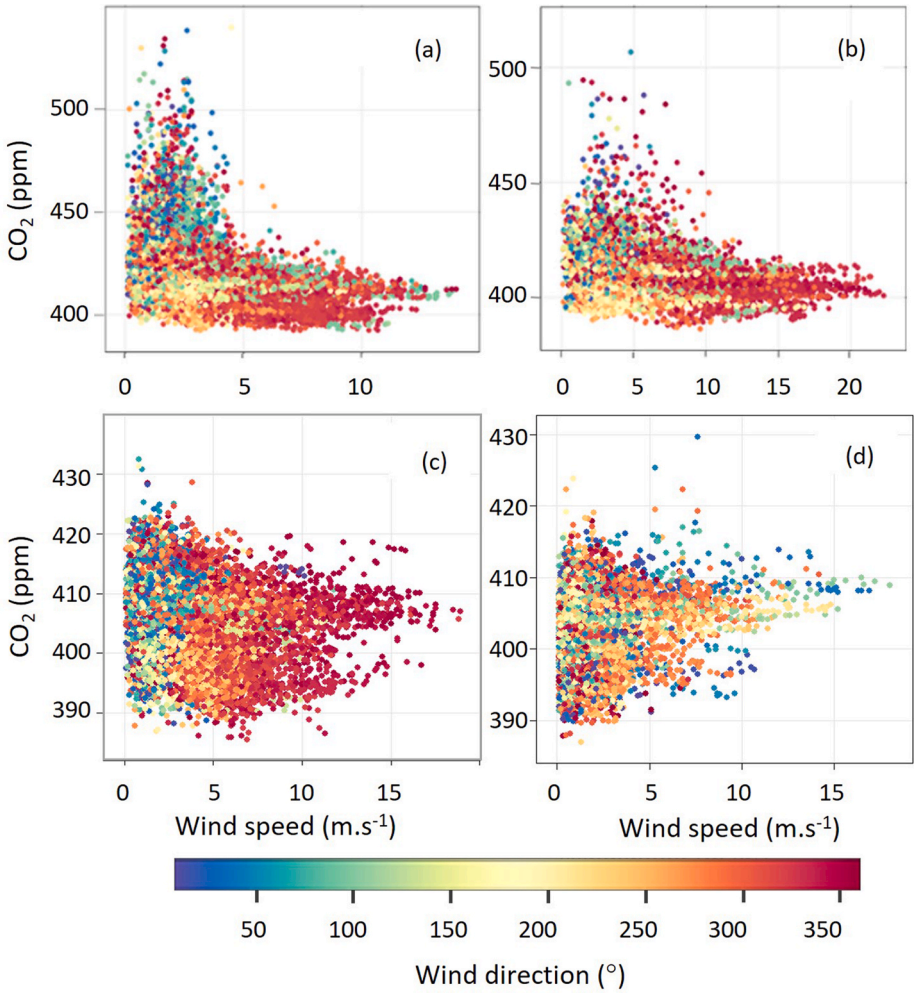

Fig. 8. (a)–(d) CO_2 hourly means at CAV, SME, OHP and ERSA, respectively, as a function of wind speed (in $m.s^{-1}$) and coloured by wind direction (in degrees). The CO_2 concentration scale is adapted for each site. The data were corrected from the annual trend at each site, interpolated by month as explained in the text.

(Fig. 9a–9d') and the associated frequency of each bin (Fig. 9a'' to Fig. 9d''). To avoid biases due to CO_2 seasonal variability (Section 3.3), the CO_2 datasets have first been seasonally adjusted according to the procedure explained in Xueref-Remy et al. (2018). Furthermore, to better assess the role of anthropogenic sources, Fig. 10 presents the CO roses obtained at ERSA, OHP and SME, and the NO_x rose at CAV, at the same bin resolution as the CO_2 roses. The scales of concentration are different from one station to another in order to adapt these figures to the range of concentration encountered at each site.

The backtrajectories (Sup. Mat. S1) show that the four stations are exposed to various wind sectors with seasonal variability (e.g. land-sea breezes during the warm seasons), as mentioned in Section 2. In order to evaluate the influence of local, regional and remote CO_2 fluxes on atmospheric CO_2, we estimate roughly the distance vs time for an airmass to integrate the different fluxes encountered on its trajectory before reaching the observation sites, taking into account wind speed and wind direction, as in Xueref-Remy et al. (2018). Indeed, at low to moderate wind speeds, the composition of an airmass observed at a given site will be dominated by atmospheric mixing of local (~10 km) to regional (~100 km) fluxes, while at high wind speeds, the local and regional fluxes will be quickly ventilated and the advection of remote fluxes will be more important.

Marseille city extends over ~10 km from its western coastal seaside to its eastern side which is enclosed by the hills of the Massif de l'Etoile. In the north Marseille is also bordered by the green hills of the Massif de l'Etoile and it extends about 20 km south to the edge of the green Massif des Calanques. Further north-west of Marseille (the distance to CAV is given in brackets), there is the Berre pond which is surrounded by anthropogenic infrastructures such as a large airport located at Marignane (~20 km); in the west-north-west coastal area is the most industrialized territory of Aix-Marseille metropolis based on oil, coal and gas combustion processes that represent more than 50% of this metropolis GHG emissions (source: www.cigale.atmosud.org), especially with La Mède area (~30 km), Lavéra area (~40 km) and Fos-sur-Mer (~50 km); this sector is also equipped with an industrial harbor for fossil fuel importations. In the north-west-north sector, petrochemical facilities are also present in Berre-l'Etang (~30 km).

Marseille city itself and the Berre pond areas are equipped with highways and national roads, supporting heavy traffic daily loads. On its seaside west/northwest of CAV, the city is set up with a touristic ferries harbor. Further north, the region is connected to the Rhone river valley, which is also industrialized, urbanized and equiped with large highways from Marseille to Lyon (~300 km). Some agricultural and natural parcels also exist in this area.

In the East sector of Marseille, the city is connected to Aubagne city (~15 km) through the Huveaune river valley, where large highway infrastructures and industrial facilities are implemented. Further east, the ground is mostly covered by forested areas.

In the south-east, there are several small cities (≤35000 inhabitants) and then Toulon city (~177 000 inhabitants) located about 40 km away, connected to Marseille through highways. Considering an air mass arriving at CAV (located a few kilometers away from the coast and

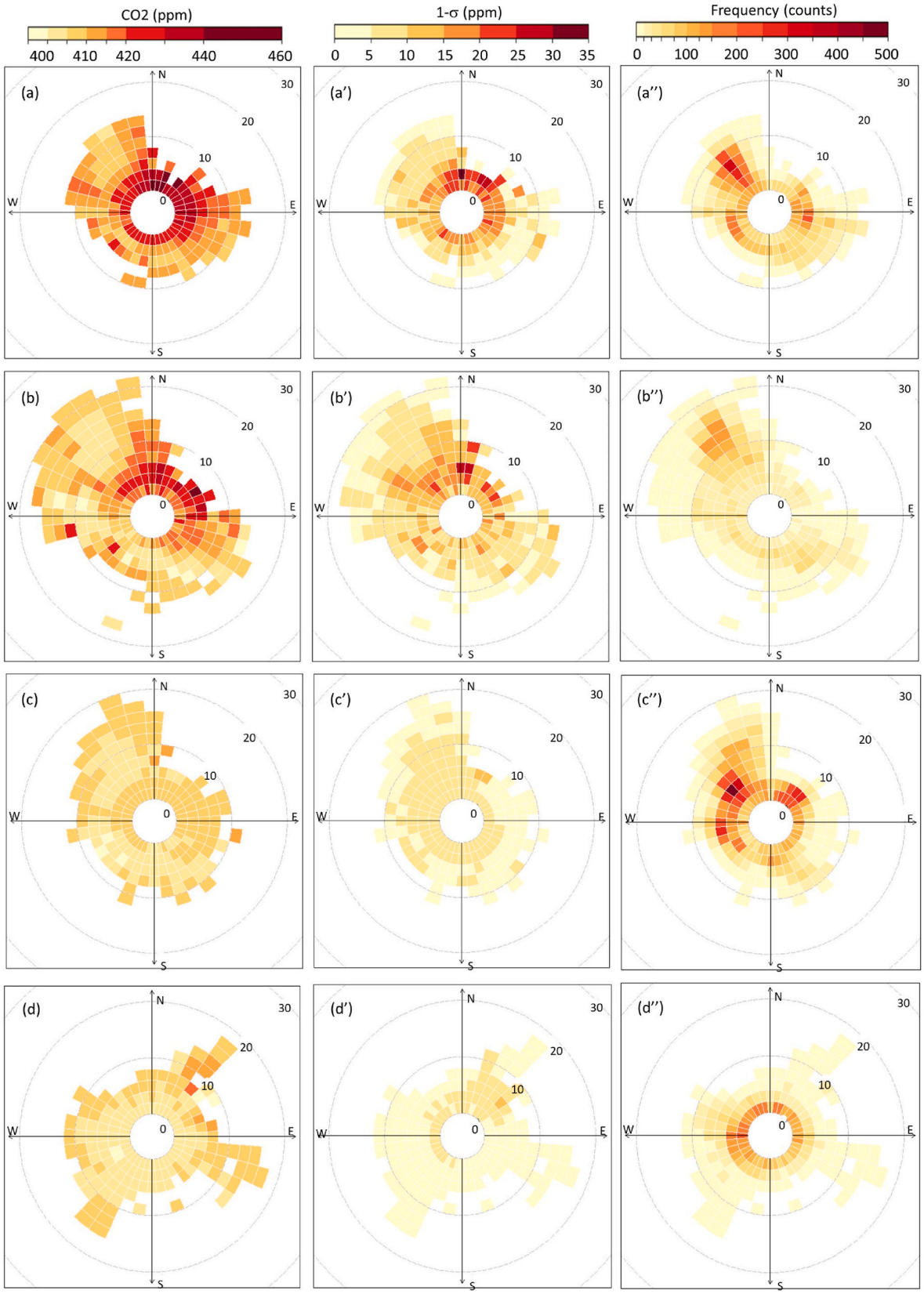

Fig. 9. (a)–(d): Mean concentrations of CO_2 at CAV, SME, OHP and ERSA respectively as a function of wind speed and direction (bins resolution: 2 km h^{-1}, 10°), with their associated standard deviation (a') to (d') and frequency of each bin (a'') to (d''), respectively. The integration is performed on the full period of the study. The data have been corrected as described in Section 3.2.

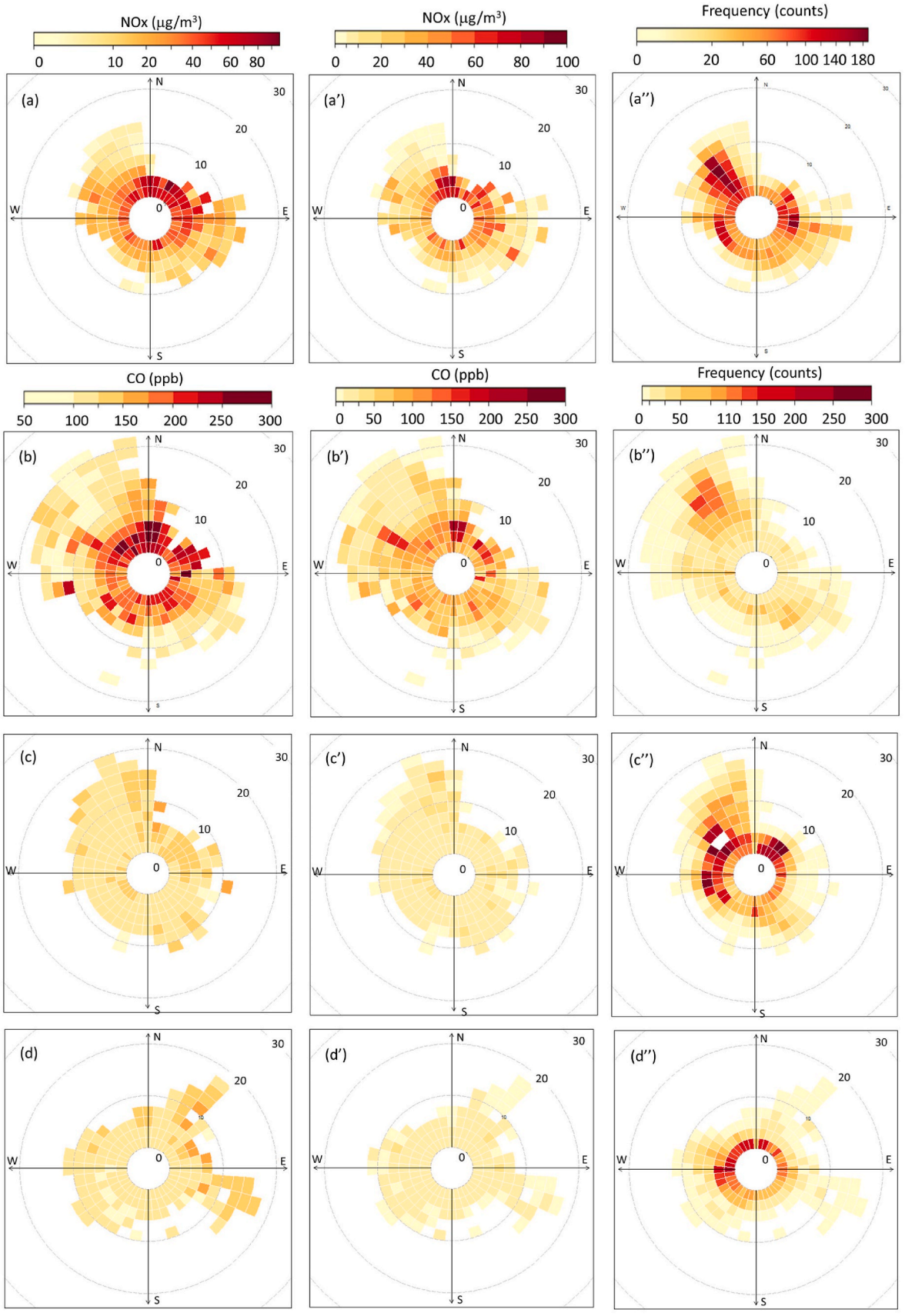

Fig. 10. Mean concentrations of (a) NOx at CAV and (b) to (d) CO at SME, OHP and ERSA, respectively, as a function of wind speed and direction (bins resolution: 2 km h^{-1}, 10°) with their associated standard deviation (a') to (d') and frequency of each bin (a") to (d"), respectively. The integration is performed on the full period of the study.

roughly in the center of the east-west axis of Marseille) at ~ 1 m s^{-1} (~4 km h^{-1}), this airmass will have stood over the city for 1 h or more, and have all that time to integrate local fluxes. An air mass arriving at CAV between roughly 1 and 4 m s^{-1} (~4 and 15 km h^{-1}) will have travelled: (1) between 15 mn only and 1h only above the city if blowing from the west; (2) between ~30 mn and ~1.5 h above the city in the east; and (3) between 40 mn and 2h in the north-south axis. Above 4 m s^{-1} (~15 km h^{-1}), any airmass will have integrated less than an hour earlier fluxes outside of the city on top of urban fluxes from Marseille city. Between 4 and 11 m s^{-1} (15–40 km h^{-1}) the airmasses will be mostly sensitive to regional fluxes from the industrial area of Berre-l'Etang in the north-west and from the Huveaune Valley and Aubagne area in the east. Above 11 m s^{-1} (40 km h^{-1}), air masses will have integrated remote fluxes, while local to regional fluxes will have been quickly ventilated by advection, poorly impacting the hourly composition of the airmass.

At SME, the situation is a bit different than at CAV, as it is exposed to the Mediterranean Sea in the west sector. Although this site can receive more « pristine » air from the sea, the atmospheric circulation pattern in the Bay of Marseille can complicate the picture: within the ESCOMPTE campaign, fine modeling studies have shown that at the time when sea breeze is getting installed, airmasses that originate from the continent pass over the Fos-Berre area before turning over the sea to reach Marseille city: this process can bring anthropogenic fluxes from this area over the city and it has been demonstrated in these cases to enrich the urban atmosphere with pollutants coming from these regional industrial sources (e.g. Drobinski et al., 2007). This process has not been studied for CO_2 yet and we will attempt to address it further below by studying the case of breezes.

At OHP, the environment is mostly rural, but as described in Section 2.1, the observatory is surrounded by small villages, cities and further the Rhone Valley, Aix-Marseille and Lyon-Grenoble metropolis that can bring remote fluxes to the station (e.g. Belviso et al., 2016; Lelandais et al., 2022) at higher wind speeds, as supported by the backtrajectories in Sup. Mat. S1.

At ERSA, the environment is mostly marine apart in the south where it is mostly rural, but the backtrajectories show that most of the airmasses arrive from the continent before reaching Corsica.

Taking this into consideration, we define three areas of influence on atmospheric CO_2 concentration at each site that we assess hereafter: local fluxes for wind speeds lower than 4 m.s^{-1} i.e. for calm, light and medium breezes as defined in Table 1 (corresponding to the threshold of the CO_2 « dome » observed on Fig. 8 for CAV and SME); regional fluxes (including more or less local fluxes) for wind speeds comprised between 4 and 10 m.s^{-1} i.e. for high breezes and medium winds according to Table 1; and remote fluxes for wind speeds higher than 10 m.s^{-1} i.e. for strong and very strong winds as defined in Table 1. Furthermore, we also take into account each bin's frequency indicating the contribution of the different areas on atmospheric CO_2. The standard deviation of each bin is an indicator of the freshness and, thus, of the proximity of the emission sources to the site, together with the corresponding CO and NOx rose bins.

3.5. Influence of remote sources

The influence of remote sources on atmospheric CO_2 is analyzed on the data corresponding to wind speed >10 m s^{-1}. For such wind speeds, CO_2 concentration variations can be analyzed in terms of background variability (i.e. without the influence of local and regional emissions). CO_2 background concentrations can vary with wind direction, as demonstrated in the Paris megacity urban CO_2 study, with differences of several ppm observed in function of wind direction because of the advection of remote anthropogenic CO_2 emissions from the Benelux and Ruhr area to Paris in the north-east sector that are not present in the other dominant wind sector blowing from the Atlantic Ocean (Xueref-Remy et al., 2018).

At CAV, wind speed higher than 10 m s^{-1} are encountered only for the two dominant wind sectors (northwest and south-east). In the northwest, the CO_2 rose shows some fine spatial variability and the CO_2 concentration varies from 400 to 420 ppm. The lowest concentrations are encountered in the 315–335° cone, with concentrations mostly in the 405–410 ppm range and a low standard deviation (<5 ppm). Upwind of CAV, this wind cone comprises the Alpilles Massif (south-east of Avignon), which seems to act as a barrier to the advection of remote emissions from the Rhone Valley. Between 275-315° and 335–355° (which bins are less frequent), the airmasses are enriched of several ppm of CO_2 as compared to the previous case. The standard deviation is lower than 5 ppm, indicating that the emissions are not fresh, and are thus remote. According to the backtrajectories, these remote emissions can arise from the Montpellier area, 200 km further in the 275–315° sub-sector, and from the Rhone valley in the 335–355° sub-sector. In the south-east and east wind sectors, wind speeds higher than 10 m s^{-1} are also not frequent and show a lower variability, ranging from 405 to 415 ppm. In this sector, backtrajectories mostly show an influence of the Mediterranean Sea. The 105–125° sub-sector shows the lowest concentration in the 405–410 ppm range such as in the 315–335° sub-sector, but they show a larger standard deviation ranging between 5 and 15 ppm, indicating the contribution of fresher and thus more proximate emissions in this sub-sector. The NOx concentrations are also higher in this direction (~10–20 μg/m^{-3}) than in the 315–335° direction (<5 μg m^{-3}). These emissions could arise from surrounding eastern cities such as Aubagne, La Ciotat and part of the urbanized coast and highways in the Toulon city area, as indicated by the backtrajectories that loop in the Aubagne-La Ciotat sector and pass over the coast. In the east sub-sector (75–105°), CO_2 ranges between 410 and 415 ppm with a higher frequency, a low standard deviation (<5 ppm) and higher NOx levels (~10–20 μg/m^{-3}) than in the 315–335° direction (<5 μg m^{-3}). This indicates the contribution of remote emissions that are quite well mixed and the impact of traffic, that could originate from the Côte d'Azur area (Nice, Monaco …) and highways located on the path of the backtrajectories; furthermore, in this wind sector airmasses are likely enriched by transboundary transport of CO_2 emissions ooming from Liguria and other areas of Italy such as the Pô river plain that are much anthropogenized and industrialized (De Feraudyet et al., 2012).

The coastal site SME is characterized by higher wind speeds than the urban site CAV because of its proximity to the sea which roughness is lower than that of the continent, and wind speeds higher than 10 m s^{-1} are more frequent. Furthermore, they cover the west to north sector as in CAV but also part of the west to south sector and the full south to east sector. Similar observations at CAV are found on the CO_2 concentrations and its variability in the north-west subsector and the east - south-east one, with the lowest concentrations also encountered in the 315–335° cone but often lower than at CAV (400–405 ppm) in the 10–18 m s^{-1} range, possibly because of the coastal position of the site that receives airmasses with a higher contribution of marine air than CAV. The standard deviation is a bit higher (5–10 ppm) than at CAV and could arise from a mix of marine and continental airmasses. The lowest CO concentrations recorded at the station are also encountered in a similar sub-sector than CAV, more precisely in the 315–325° sub-sector.

For winspeeds higher than 18 m s^{-1} winds come from the NNE sector. Concentrations are more elevated (405–410 ppm) in the same range as CAV and characterized by a lower standard deviation (<5 ppm) which indicates that they come from well-mixed remote airmasses as in CAV, although not heavily charged in anthropogenic emissions, possibly because of the presence of the Alpilles Massif upwind in this direction. Concentrations are more variable in the 275–315° and 335–355° sub-sectors as in CAV, ranging from 395 to 420 ppm and a standard deviation standing between 0 and 15 ppm: these sub-sectors are likely influenced by the advection of marine air but also by remote emissions, likely from Montpellier and the Rhone Valley, as in CAV.

In the south-east and south sector (115°–205°), the CO_2 variability at high wind speed is a bit lower than in the north-west one, with concentrations ranging between 400 and 410 ppm as in the 105–125° sector

for CAV. The backtrajectory clusters show a strong influence of the Mediterranean Sea in these wind directions. Similar concentrations are encountered in the 315–345° sector at SME and in the 315–335° at CAV. In the 135–195° sub-sector, the standard deviation is the lowest (<5 ppm) and the concentration is always in the 405–410 ppm range, which indicates well-mixed air masses and some contribution of remote emissions, likely from Italy (De Feraudyet et al., 2012), as also supported by the backtrajectories, especially in Summer (cluster 1). The east sub-sector (85–105°) is characterized by a wider range of concentrations (400–420 ppm) and higher standard deviation levels (0–15 ppm). This indicates, similarly to CAV the presence of a contribution of fresher emissions from cities in the vicinity of Marseille, such as Aubagne and the anthropogenized coastal area East of Marseille, as supported by the backtrajectories (Suppl. Mat. S1).

At OHP, distant sources of CO_2 can impact OHP by the advection of CO_2-enriched air masses (as shown by the presence of spikes on the timeseries, such as in Dec. 2014). Such advections of anthropic plumes up to this site have already been demonstrated for some urban and industrial pollutants (Gaudel et al., 2015; Belviso et al., 2016) but also for CO_2 for which they represent some percents of the data collected at OHP (Lelandais et al., 2022). Most of the bins with wind speeds higher than 10 m s^{-1} are in the north-west/north direction and range from 400 to 410 ppm. In this direction, the highest concentrations are encountered in the 335°–5° sub-sector and the lowest in the 315°–335° one. In each wind cone, the highest the wind speed is, the lowest the standard deviation is, ranging low between 0 and 10 ppm, indicating well-mixed air masses.

The hourly mean CO concentration behaves similarly, as does its standard deviation (ranging from 125 to 150 ppb/25–75 ppm in the first sub-sector and from 100 to 125 ppb/10–25 ppb in the second sub-sector for the concentration and the standard deviation, respectively). According to the backtrajectories (Sup. Mat. S1), the higher CO_2 and CO concentrations from the 335°–5° subsector can be explained by the advection of CO_2 emissions from the Rhone valley and Lyon city, located about 200 km further north-north-east of OHP, and alpine cities such as Gap and Grenoble (Lelandais et al., 2022). In the other wind sectors and for wind speed higher than 10 m s^{-1}, one bin shows higher CO_2 concentration (410–415 ppm) with low standard deviations (<5 ppm), in the east (95–105°) direction, but these are rare as indicated by the bins frequency. These are associated with higher CO levels (150–175 ppb) with low standard deviations (<10 ppb) indicating the ponctual influence of remote sources, respectively, from the Côte d'Azur and possibly Italy, and the Aix-Marseille metropolis as indicated by the backtrajectories.

At ERSA, wind speeds higher than 10 m s^{-1} are not frequent and occur in the NE, ESE, SW and in a less extend in the W and WNW. In almost all cases, the CO_2 standard deviation is low (<5 ppm), indicating well-mixed air masses. CO_2 ranges between 400 and 415 ppm, the highest concentrations being encountered in the NE (25–45°) but are not much occurrent. As for CO_2, higher CO concentrations are associated with the NE sector, followed by the SE one (125–175 ppb against 100–125 ppb in the other sectors). The backtrajectories indicate that the NE higher concentrations are likely due to the integration of atmospheric emissions from the continental Italian boot where large anthropogenic sources exist (e.g. Roma, Genova, La Spezia, Torino, the Pô river plain …).

3.6. Influence of regional fluxes

The influence of regional emissions is analyzed using the bins for which wind speed is comprised between 4 and 10 m s^{-1}.

At CAV, the influence of regional emissions can be seen in specific directions where CO_2 and NOx concentrations range in the higher concentration levels encountered at this site. These directions are mostly N (335-5°), NNE (15–25°), NE to ESE (45–125°), S and SW (185–195° and 215–235°), W (255–265°) and WNW (285–295°), and occur mostly for wind speed comprised between 4 and 8 m s^{-1}. In the N and NNE sectors, there is likely an influence of regional sources such as traffic from the A51 highway, as well small cities with nearby industrial sources such as Septèmes-les-Vallons, Simiane-Colombes, Bouc-Bel-Air and even Gardanne, located just behind the Massif de l'Etoile, which emissions could be transported by airmasses along the backtrajectories shown in Suppl. Mat. S1. As mentioned above, Gardanne owns one of the four last thermal plants of France (20 km north of CAV), which is known to be a large CO_2 emitter point source, based mostly on coal combustion and partly on wood burning and equipped with several chimneys among which the highest in France (297 m AGL, ~500 m ASL). Plumes emitted by this facility could be transported above the Massif de l'Etoile (elevation ~ 550–600 m ASL in the Gardanne-CAV axis, https://fr-fr.topographic-map.com/maps/gp/Marseille/) and to the city by catabatic winds. The resolution of our backtrajectories is too low to confirm or infirm this hypothesis, but it would be interesting to further investigate on this point within a dedicated modeling study. In the NE to ESE sectors, CAV is likely exposed to emissions from the Huveaune valley and closeby cities (residential and industrial activities, A50 highway, Aubagne and Gemenos cities …). In the S and SW sectors, regional sources could be regular ferries which pass in the Bay at a distance of 15–20 km from CAV. We likely see the impact of emissions from ferries and industrial sources transported from the Fos-Berre area to the site in the W and WNW sectors.

At SME, for wind speeds comprised between 4 and 10 m s^{-1}, higher CO_2 and CO concentrations are encountered in the NW to NNE sector (315°–35°), in the NE to E (35–95°), in the SSW to SW (195–245°, especially for CO), in the W (165–175°) and in the WWN (195–215°). There are large and highly variable signals in the N, reaching 440 ± 35 ppm for CO_2 and 300 ± 300 ppb for CO. Such signals indicate the contribution of large urban/industrial regional sources from that wind sector as in CAV but not constantly, probably from the position of the site on the littoral and the mixing of continental and marine air in this direction. In the NE to E, the regional sources contributing to SME signals are likely as for CAV. There is probably an impact of regular ferry lines in the Bay as for CAV in the SSW to SW. These higher signals occur only during daytime, which conforts our hypothesis. In the W and WWN, we likely see the impact of the Fos-Berre area.

At OHP, regional signals are quite weak and stand between 400 and 415 ppm for CO_2 and between 100 and 175 ppb for CO, and occur mostly from the WSW and NW sectors. Less frequent, the highest concentrations are encountered in the N and NE to E. The maxima in the N direction are likely due to emissions advected from the A51 highway and cities along this latter, such as Sisteron. In the SE and ENE directions, cities in the Durance valley and traffic on the A51 highway located in this valley (~10–30 km away from OHP) are likely the primary sources contributing to these regional signals, although not much frequent. A deeper insight of atmospheric CO_2 variability at the OHP site is given in Lelandais et al. (2022).

At ERSA, most of the bits for wind speed between 4 and 10 m s^{-1} stand within 405 and 420 ppm for CO_2 and 100–175 ppb for CO. The highest concentrations are encountered in the NE (although not frequently), followed mainly by the ENE, NW and W sectors. These higher signals could arise from plumes emitted by regular ferries sailing from France and Italy to Corsica and vice-versa, which lines pass along the N, E and W coasts of Corsica at a distance of ~15–20 km for most of them, but also further.

3.7. Influence of local emissions

At CAV, the influence of local emissions is visible in all wind directions for wind speeds lower than 2 m s^{-1}, as CO_2 concentrations are enriched of several ppm to several tens of ppm (ranging between 415 and 460 ppm) in comparison with regional background concentrations (400–410 ppm). This influence is also visible between 2 and 4 m s^{-1} but with higher variability function of wind direction, which is more

established at such wind speeds. In such conditions, the CO_2 concentration varies between 405 and 460 ppm. The highest CO_2 concentrations between 0 and 2 m s^{-1} and 2–4 m s^{-1} are associated to winds from the north and north-east (355°–25° and 15°–45°, respectively), with a high frequency as well as a high standard deviation (15–25 ppm and 20–35 ppm, respectively) which indicates fresh emissions i.e. the influence of sources relatively close to the site, such as traffic on boulevards. On the west side, activities related to Marseille harbour and ferries likely contribute to the local signals received at CAV. Similar patterns are observed on the NOx rose, which indicates the influence of anthropogenic sources and especially traffic as one of the major local sources impacting the station as expected and mostly in the northwest to the southeast in the 2–4 m s^{-1} range (with concentration ranging between 30 and 90 μg m^{-3} and a maximum of 90 μg m^{-3} in the 30–40° wind subsector), and in almost all directions in the 0–2 m s^{-1} one with higher levels in the northwest to east sectors (40–80 μg m^{-3}).

At SME, the influence of local sources is spatially more heterogeneous than at CAV. Concentrations are higher in the 300°–160° sector ie from the NW to the SE (420–440 ppm range), especially for wind speed comprised between 2 and 4 m s^{-1}. The lowest concentrations are encountered in the SW sector. The local regime of breezes partly controls this spatial variability, as further inferred here below. CO concentrations follow a similar pattern with the lowest concentrations in the SW ranging between 125 and 200 ppb - which are a bit higher than concentrations encountered for remote signals (50–100 ppb) - and the highest concentrations in the NW to SE ranging between 200 and 300 ppb. Enriched CO concentrations, relatively to background ones, can be explained by the contribution of anthropogenic sources. The standard deviation is also higher for local signals than remote ones, reaching values as large as 200 ppb which indicates the contribution of nearby sources to the site, even for the sector exposed to the Bay of Marseille. SME is situated on the littoral, which exposes this station either to nearby urban sources from Marseille city (traffic, heating but also emissions from Marseille harbour activities and ferries in the N/NE), or to marine air mixed partly with anthropogenic emissions, possibly from ferries (and the Frioul islands in the W) in the Bay of Marseille, and from the remainings of urban and industrial plumes of Marseille and Fos-Berre areas.

At OHP, for wind speeds lower than 4 m s^{-1} CO_2 is mostly in the 405–410 ppm range, which is a bit higher than remote signals. The standard deviation is also a bit higher, mostly between 5 and 10 ppm, indicating the contribution of fresher emissions. The CO rose indicates that there are some local sources that influence the station such as villages (e.g. Saint-Michel-l'Observatoire, Reillane in the SW; Limans, Revest-des-Brousses in the N and NNE) and small cities (e.g. Mane, Forcalquier in the NE and E). This was deeply inferred in Lelandais et al. (2022) which showed that local sources (mostly traffic and residential heating) impacted less than 5% of the data collected at this station.

At ERSA, for wind speeds less than 4 m s^{-1}, the CO_2 concentration is quite stable in all wind sectors, standing on average within 400–405 ppm with a few bits only ranging in the 405–410 ppm, mainly in the NE. CO ranges mostly between 100 and 125 ppb and there are only a few bits on the CO roses showing higher CO concentrations in the NE, ranging between 125 and 150 ppb, which is still low in comparison to local urban signals such as the ones received at SME. The standard deviation is also much lower and indicates that the influence of local sources is poor. The sparse higher concentrations encountered in the NE are likely due to plumes of sources located further away.

3.7.1. *Influence of a local meteorological feature in Marseille: NE land/SW sea breezes*

In the Marseille city, the CO_2 roses (Fig. 9) show that the NE sector is most often characterised by higher concentrations than the SW sector. These wind sectors are characteristic of well established land/sea breezes, for wind speed below 6 m s^{-1}. Breeze regimes have been studied within the ESCOMPTE program (e.g. Bastin et al., 2005; Drobinski et al., 2007), as well as their impact on the variability of some pollutants, but never on atmospheric CO_2 and only for the Summer season. Our meteorological dataset indicates that breezes accounted for a few percents of winds from the SW sector (sea breezes) and from the NE sector (land breezes) during the period of study.

To deeper infer the role of NE/SW breezes on atmospheric CO_2 in Marseille, we analyse the normalized and seasonally adjusted mean diurnal cycles of CO_2 by season on the SME site, in the conditions of NE land/SW sea breeze processes for wind speed comprised between 2 and 6 m s^{-1} (Fig. 11). The number of observations available to calculate each hourly means is also displayed. Let us recall that there is no data available for Spring at this station. While breezes are thermally driven and occur in Marseille mostly in Summer, Fig. 11 show that they also occur in the other seasons. Furthermore, in Winter land breezes start in the late evening, while in Summer they start later in the middle of the night. A NE land breeze is observed between 21h00 and 08h00 in wintertime, and between 02h00 and 07h00 in the summertime. Later then, when the continent has warmed up, the sea breeze sets up and a slow SW wind is established in Summer mostly during daytime, between 10h00 and 22h00; in Winter, sea breezes are also observed from that wind sector but they are shorter and occur only in the late afternoon/early evening, from 18h00–22h00. SE and NW breezes are also observed in Autumn with an intermediate duration compared to Summer and Winter.

Fig. 11 shows how the land/sea breezes regime modulates atmospheric CO_2 along the day at SME, on the littoral of Marseille. In Summer, in NE land breeze conditions, atmospheric CO_2 is about 10 ppm above the mean diurnal cycle concentration, whereas it stands about 3 ppm lower than this mean when SW sea breezes are stabilized. During the winter, the difference of CO_2 concentration between the two breeze regimes can reach 40 ppm. When the SW sea breeze is set up, atmospheric CO_2 concentrations (Fig. 11) are in all seasons several ppm lower than during land breeze events. Indeed, in a situation of NE land breeze, air masses pass over Marseille city before arriving at SME and are thus enriched in CO_2 from the urban anthropogenic emissions. Moreover, land breezes occur at night when the atmospheric boundary layer is the lowest of the day, contrary to sea breezes which occur during daytime when the boundary layer is the most developed. Both of these factors generate higher CO_2 concentrations at SME in NE land breeze conditions than during SW sea breeze ones. This effect is not only visible on the CO_2 roses at SME, but also at CAV (Fig. 9). Thus, when the wind blows from the SW sector, the concentrations are lower, since the air coming from the sea is usually not loaded with local/regional emissions - apart in some specific situations (e.g. transport of CO_2 plumes from the Fos-Berre

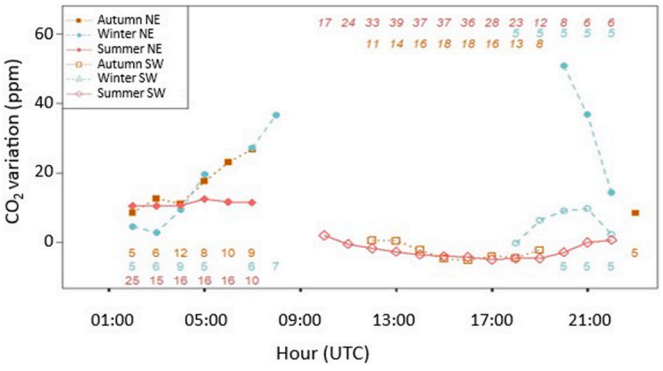

Fig. 11. Mean diurnal cycles of CO_2 for each season (but Spring) during NE land breeze (plain symbols) and SW sea breeze (empty symbols) regimes at the SME station. The data were corrected from the CO_2 annual trend of the site and seasonally normalized. Wind speed is comprised between 2 and 6 m s^{-1}. The number of observations associated to each hourly mean is displayed and coloured accordingly to the corresponding season, as given in the top left corner. There is no data in Spring at SME due to successive instrumental failures.

industrial area). The contrast is even stronger in Autumn and in Winter, since Marseille's anthropogenic emissions are more substantial during these two seasons than in Summer due to the heating sector's emissions, and the winter's atmospheric boundary layer is the thinnest of the year. However, in Winter, SE breezes show higher CO_2 concentration levels (until ~10 ppm more) than in the other seasons: this can be explained by the impact of anthropogenic emissions from Marseille and/or Fos areas diluting in the shallow ABL and transported by land breezes over the sea bay during nighttime, then brought back over the continent by sea breezes during daytime (e.g. Drobinski et al., 2007).

In some cases, the number of observations used to calculate the cycles of Fig. 11 is quite low - and even inexistent for the Spring season. More data would be useful to get a deeper quantification of the impact of breezes on CO_2 in Marseille in all seasons.

4. Conclusion

In the present study, we analyzed for the first time the variability of atmospheric CO_2 in the area of the Marseille city (France) in the North-West Mediterranean Basin, through the analysis of in-situ observations of CO_2, CO and NOx collected at four sites, two of them being located in the urban center and on the coast of Marseille (in collaboration with the regional air quality monitoring agency ATMOSUD), and the two others being regional background sites located at the Observatoire de Haute Provence (80 km north of Marseille) and at Cape Corsica (belonging to the ICOS-France national atmospheric greenhouse observation network). The period of observation was comprised between 2013 and 2018, depending on each site and the analysis was mostly made on the period common to all sites (1 July 2016–13 February 2018).

At the four sites, the CO_2 growth rate was found to be of the same order of magnitude than the reference site of the northern hemisphere, Mauna Loa (Hawaii). However, CO_2 concentrations are enriched of several ppm at both urban sites due to their proximity to anthropogenic emissions and especially in the city center, ranging on average from 411.7 ± 13.8 ppm on the coast of Marseille to 423.9 ± 17.6 ppm in the city center, as compared to both background sites (409.1 ± 6.5 ppm inland at OHP, ~80 km north of Marseille, and 406.3 ± 6.0 ppm at the Cape Corsica marine site). As found in previous CO_2 urban studies, the amplitude of the diurnal cycle, partly driven by the ABLH cycle on the continental sites (not at the marine background site), is much higher at the urban sites (ranging from 14.5 ppm on the city coast to 18.8 ppm in the city center) because of their proximity to large anthropogenic emissions (mostly from traffic and heating) than at both background sites (from 0.5 ppm at the marine site to 5.3 ppm at the rural site): these latters are mainly influenced by natural fluxes with only a small influence of local, regional and remote anthropogenic emissions. There is almost no diurnal variation of CO_2 at Cape Corsica, which is strongly under the influence of the small CO_2 fluxes exchanged between the atmosphere and the Mediterranean Sea, while the diurnal variation at OHP are larger, especially below 50 m AGL, because they are driven by the exchanges between the continental biosphere and the atmosphere, and ABLH dynamics. Similarly, the amplitude of the CO_2 seasonal cycle is higher in the city (29.2 ppm in the urban center and 20.3 ppm on the urban coast, respectively) than at the continental background site (13.1 ppm) and at the marine background site (13.9 ppm); on the continent, this cycle is mostly driven by the seasonal variability of the ABLH but also by the seasonality of anthropogenic emissions (heating mostly) in the city and of the activity of the surrounding vegetation at the Observatoire de Haute Provence.

A strong dependance of CO_2 on wind conditions is found at both urban sites, in agreement with other urban studies. Atmospheric CO_2 forms a dome of several tens of ppm at low wind speed above the city in comparison to the background sites. A CO_2 gradient of several ppm between the 4 sites still exists for mid wind speed. The amplitude of the gradient depends also on the wind direction. Especially, the influence of remote emissions on atmospheric CO_2 in the studied area is variable with wind direction, with differences of concentration of a few ppm in the background stations to more than 10 ppm in the urban ones.

While our study shows that our background sites can be relevant to address the regional variability of CO_2, additional sites are needed to better constrain the Marseille CO_2 urban plume, with upwind background stations located a few kilometers away from the city only and on the path of the dominant winds, especially in the NW sector where the remote signals are more variable and sometimes several ppm higher than the ones received by our background sites. In the W sector as well, Marseille can receive industrial CO_2 plumes from Fos-Berre, where new observation sites should be implemented to better constrain the background levels upwind of the city and for a better understanding of the CO_2 variability in this strongly anthropogenized area. Finally, implementing new sites in the area of Aix-en-Provence would allow an analysis of atmospheric CO_2 on the full territory of the Aix-marseille-Provence metropolis. The local land/sea breeze regime, although not much frequent, is also shown to control atmospheric CO_2 in Marseille by increasing the urban CO_2 concentration of several tens of ppm in land breeze conditions as compared to sea breeze ones, with a dependency on the season. Dedicated meteorological stations would be a plus to better characterize the breezes variability and its impact on atmospheric CO2 in Marseille.

To deeper address the role of anthropogenic vs natural fluxes, as well as the different emission sectors (including biomass burning) on atmospheric CO_2 in the Aix-Marseille-Provence metropolis area in order to assess the CO_2 emissions inventory independently, measurements of carbon isotopes and tracers such as carbone monoxide, nitrogen oxydes, black carbon and volatil organic compounds need to be further developed at the different sites. Finally, as wind conditions and the ABLH both partly controls atmospheric CO_2 at the diurnal, synoptic and seasonal scale, a continuous monitoring of these parameters in and out of the city which is curently under development through the ANR COoL-AMmetropolis project will soon be of great help to complete our regional observation network in this strongly urbanized and industrialized coastal area.

CRediT authorship contribution statement

Irène Xueref-Remy: conception and design of the work, data collection, data analysis and interpretation, drafting the article, critical revision of the article. **Mélissa Milne:** data analysis and interpretation, drafting the article, critical revision of the article. **Narimène Zoghbi:** data analysis and interpretation, critical revision of the article. **Ludovic Lelandais:** drafting the article, critical revision of the article. **Aurélie Riandet:** drafting the article, critical revision of the article. **Alexandre Armengaud:** data collection. **Grégory Gille:** data collection. **Ludovic Lanzi:** data collection. **Sonia Oppo:** data collection, data analysis and interpretation. **Lola Brégonzio-Rozier:** data collection, critical revision of the article. **Pierre-Eric Blanc:** data collection. **Christophe Yohia:** data collection. **Jacques Piazzola:** data analysis and interpretation. **Marc Delmotte:** data collection, critical revision of the article.

Declaration of competing interest

The authors declare that they have no known competing financial interests or personal relationships that could have appeared to influence the work reported in this paper.

Data availability

Data will be made available on request.

Acknowledgments

This work was financed by the LABEX OT-MED Aix-Marseille Carbon Pilot Study (AMC) project and the COoL-AMmetropolis project funded

by the Agence National de la Recherche (grant number ANR-19-CE03-0008) and supported through the Service National d'Observation ICOS-RAMCES of CNRS and the ATMOSUD regional air quality agency. The authors thank the SIP (Service Informatique PYTHEAS) for their technical support. We acknowledge M. Ramonet, L. Hazan and D. Combaz from the ICOS-RAMCES network for providing us the ERSA data and for technical support at OHP. The authors thank the ATMOSUD technical team and especially L. Lanzi for their technical support at the CAV (Marseille Longchamp) station. We are grateful to M. Fornier and M. Lafond for their technical help at the Station Marine d'Endoume (SME). The authors gratefully acknowledge the NOAA Air Resources Laboratory (ARL) for the provision of the HYSPLIT transport and dispersion model and/or READY website (https://www.ready.noaa.gov) used in this publication. We thank the R – OpenAir package creators for providing such useful open sources analysis tools.

Appendix A. Supplementary data

Supplementary data to this article can be found online at https://doi.org/10.1016/j.aeaoa.2023.100208.

References

Ammoura, L., Xueref-Remy, I., Gros, V., Baudic, A., Bonsang, B., Petit, J.-E., Perrussel, O., Bonnaire, N., Sciare, J., Chevallier, F., 2014. Atmospheric measurements of ratios between CO_2 and co-emitted species from traffic: a tunnel study in the Paris megacity. Atmos. Chem. Phys. 14, 12871–12882. https://doi.org/10.5194/acp-14-12871-2014.

Ammoura, L., Xueref-Remy, I., Vogel, F., Gros, V., Baudic, A., Bonsang, B., Delmotte, M., Té, Y., Chevallier, F., 2016. Exploiting stagnant conditions to derive robust emission ratio estimates for CO_2, CO and volatile organic compounds in Paris. Atmos. Chem. Phys. 16, 15653–15664. https://doi.org/10.5194/acp-16-15653-2016.

Banks, R.F., Tiana-Alsina, J., Baldasano, J.M., Rocadenbosch, F., Papayannis, A., Solomos, S., Tzanis, C.G., 2016. Sensitivity of boundary-layer variables to PBL schemes in the WRF model based on surface meteorological observations, lidar, and radiosondes during the HygrA-CD campaign. Atmos. Res. 176–177 https://doi.org/10.1016/j.atmosres.2016.02.024.

Bastin, S., Drobinski, P., Dabas, A., Delville, P., Reitebuch, O., Werner, C., 2005. Seabreeze case study using a combination of observations and numerical simulation in complex terrain in souhtern France: contribution to mass transport. In: 6th ESCOMPTE Workshop, Feb 2005, Marseille, France ffhal-00142148f. https://hal.archives-ouvertes.fr/hal-00142148/document.

Belviso, S., Reiter, I.M., Loubet, B., Gros, V., Lathière, J., Montagne, D., d Delmotte, M., Ramonet, M., Kalogridis, C., Lebegue, B., Bonnaire, N., Kazan, V., Gauquelin, T., Fernandez, C., Genty, B., 2016. A top-down approach of surface carbonyl sulfide exchange by a Mediterranean oak forest ecosystem in southern France. Atmos. Chem. Phys. 16 (2016), 14909–14923. https://doi.org/10.5194/acp-16-14909-2016.

Brahmanandam, P.S., KuCAV, V.N., KuCAV, G.A., Rao, M.P., Samatha, K., Ram, S.T., 2020. A few important features of global atmospheric boundary layer heights estimated using COSMIC radio occultation retrieved data. Indian J. Phys. 94 (2020), 555–563. https://doi.org/10.1007/s12648-019-01514-7.

Bréon, F.M., Broquet, G., Puygrenier, V., Chevallier, F., Xueref-Remy, I., Ramonet, M., Dieudonné, E., Lopez, M., Schmidt, M., Perrussel, O., Ciais, P., 2015. An attempt at estimating Paris area CO_2 emissions from atmospheric concentration measurements. Atmos. Chem. Phys. 15, 1707–1724. https://doi.org/10.5194/acp-15-1707-2015.

Conil, S., Helle, J., Langrene, L., Laurent, O., Delmotte, M., Ramonet, M., 2019. Continuous atmospheric CO_2, CH_4 and CO measurements at the Observatoire Pérenne de l'Environnement (OPE) station in France from 2011 to 2018. Atmos. Meas. Tech. 12 (2019), 6361–6383. https://doi.org/10.5194/amt-12-6361-2019.

De Feraudyet, P., Bernard, M., Chevalier, L., Gille, G., Luneau, G., Peron, F., Rocher, B., Souweine, R., Virga, J., Armengaud, A., 2012. Estimations des interactions atmosphériques entre les régions PACA et Ligurie, Projet Stratégique AERA : Air Environnement Régions ALCOTRA 2007-2013, Projet : 11ETU11E - Action Pilote 5.5.6 - AirPACA, p. 56. Décembre 2012. https://www.atmosud.org/sites/paca/files/publications_import/files/121200_AirPACA_AERA_interactions_franco_Ligure_net.pdf.

Delmotte, M., Ramonet, M., Kazan, V., Vuillemin, C., Combaz, D., Hego, L., El Yazidi, A., Laurent, O., Lebègue, B., Xueref-Rémy, I., Yver-Kwok, C., Blanc, P.E., Conil, S., Gheusi, F., Pichon, J., Paris, J.D., Ciais, P., 2015. The French metropolitan greenhouse gases monitoring network : SNO-ICOS France, 18th WMO/IAEA meeting on carbon dioxide, other greenhouse gases, and related measurement techniques (GGMT), SCRIPPS institution of oceanography. La Jolla, Sept. 13-17, 2015, Abstract # B22. https://cme.ucsd.edu/ggmt-2015/GGMT%20FINAL%20ABSTRACT%20BOOK%202015.pdf.

Draxler, R.R., 1999. HYSPLIT4 User's Guide, *NOAA Tech. Memo* ERL ARL-230. NOAA Air Resources Laboratory, Silver Spring, Md, USA.

Drobinski, P., Bastin, S., Dabas, A.M., Delville, P., Reitebuch, O., 2006. Variability of the three-dimensional sea-breeze structure in southeastern France: observations and evaluation of empirical scaling laws. Ann. Geophys. 24, 1783–1799.

Drobinski, P., Saïd, F., Ancellet, G., Arteta, J., Augustin, P., Bastin, S., Brut, A., Caccia, J. L., Campistron, B., Cautenet, S., Colette, A., Coll, I., Corsmeier, U., Cros, B., Dabas, A., Delbarre, H., Dufour, A., Durand, P., Guénard, V., Hasel, M., Kalthoff, N., Kottmeier, C., Lasry, F., Lemonsu, A., Lohou, F., Masson, V., Menut, L., Moppert, C., Peuch, V.H., Puygrenier, V., Reitebuch, O., Vautard, R., 2007. Regional transport and dilution during high-pollution episodes in southern France: summary of findings from the field experiment to constraint models of atmospheric pollution and emissions transport (ESCOMPTE). J. Geophys. Res. 112, D13105 https://doi.org/10.1029/2006JD007494.

Drobinski, P., Bastin, S., Arsouze, T., Beranger, K., Flaounas, E., Stéfanon, M., 2018. North-western Mediterranean sea-breeze circulation in a regional climate system model. Clim. Dynam. 51 (3), 1077–1093. https://doi.org/10.1007/s00382-017-3595-z.

François, S., Grondin, E., Fayet, S., Ponche, J.L., 2005. The establishment of the atmospheric emission inventories of the ESCOMPTE program. Atmos. Res. 74, 5–35. https://doi.org/10.1016/j.atmosres.2004.10.002.

Friedlingstein, Pierre, O'Sullivan, Michael, Jones, Matthew, W., Andrew, Robbie M., Hauck, Judith, Olsen, Are, Peters, Glen P., Peters, Wouter, Pongratz, Julia, Sitch, Stephen, Le Quéré, Corinne, Canadell, Josep, G., Ciais, Philippe, Jackson, Robert B., Alin, Simone, Aragão, Luiz E.O. C., Arneth, Almut, Arora, Vivek, Bates, Nicholas R., Becker, Meike, Benoit-Cattin, Alice, Bittig, Henry C., Bopp, Laurent, Bultan, Selma, Chandra, Naveen, Chevallier, Frédéric, Chini, Louise P., Evans, Wiley, Florentie, Liesbeth, Forster, Piers M., Gasser, Thomas, Gehlen, Marion, Gilfillan, Dennis, Gkritzalis, Thanos, Gregor, Luke, Gruber, Nicolas, Harris, Ian, Hartung, Kerstin, Haverd, Vanessa, Houghton, Richard A., Tatiana, Ilyina, Jain, Atul K., Joetzjer, Emilie, Kadono, Koji, Kato, Etsushi, Kitidis, Vassilis, Korsbakken, Jan, Ivar, Landschützer, Peter, Lefèvre, Nathalie, Lenton, Andrew, Lienert, Sebastian, Liu, Zhu, Lombardozzi, Danica, Marland, Gregg, Metzl, Nicolas, Munro, David R., Nabel, Julia E.M. S., Nakaoka, Shin-Ichiro, Niwa, Yosuke, O'Brien, Kevin, Ono, Tsuneo, Palmer, Paul, I., Pierrot, Denis, Poulter, Benjamin, Resplandy, Laure, Robertson, Eddy, Rödenbeck, Christian, Schwinger, Jörg, Séférian, Roland, Skjelvan, Ingunn, Smith, Adam, J.P., Sutton, Adrienne J., Tanhua, Toste, Tans, Pieter P., Tian, Hanqin, Tilbrook, Bronte, van der Werf, Guido, Vuichard, Nicolas, Walker, Anthony, P., Wanninkhof, Rik, Watson, Andrew J., Willis, David, Wiltshire, Andrew J., Yuan, Wenping, Yue, Xu, Zaehle, Sönke, 2020. Global carbon budget 2020. Earth Syst. Sci. Data 12, 3269–3340. https://doi.org/10.5194/essd-12-3269-2020.

Gratani, L., Varone, L., 2005. Daily and seasonal variation of CO_2 in the city of Rome in relationship with the traffic volume. Atmos. Environ. 39, 2619–2624. https://doi.org/10.1016/j.atmosenv.2005.01.013.

Grimmond, C.S.B., Salmond, J.A., Oke, T.R., Offerle, B., Lemonsu, A., 2004. Flux and turbulence measurements at a densely built-up site in Marseille: heat, mass (water and carbon dioxide), and momentum. J. Geophys. Res. 109, D24101 https://doi.org/10.1029/2004JD004936, 2004.

Guenard, V., Drobinski, P., Caccia, J.L., Campistron, B., Benech, B., 2005. An observational study of the mesoscale mistral dynamics. Boundary-Layer Meteorol. 115, 263–288, 2005.

Hazan, L., Tarniewicz, J., Ramonet, M., Laurent, O., Abbaris, A., 2016. Automatic processing of atmospheric CO_2 and CH_4 mole fractions at the ICOS atmosphere thematic Centre. Atmos. Meas. Tech. 9, 4719–4736. https://doi.org/10.5194/amt-9-4719-2016, 2016.

Idso, C.D., Idso, S.B., Balling Jr., R.C., 2001. An intensive two-week study of an urban CO_2 dome in Phoenix, Arizona, USA. Atmos. Environ. 35, 995–1000. https://doi.org/10.1016/S1352-2310(00)00412-X.

Idso, S.B., Idso, C.D., Balling Jr., R.C., 2002. Seasonal and diurnal variations of near-surface atmospheric CO_2 concentration within a residential sector of the urban CO_2 dome of Phoenix, AZ, USA, Atmos. Environ. Times 36, 1655–1660. https://doi.org/10.1016/S1352-2310(02)00159-0-2002.

IEA, 2017. CO_2 Emissions from Fuel Combustion. Oveview, 2017. http://www.iea.org/publications/freepublica-tions/publication/CO2EmissionsFromFuelCombustion2017Overview.pdf.

IPCC, 2013. In: Stocker, T.F., Qin, D., Plattner, G.-K., Tignor, M., Allen, S.K., Boschung, J., Nauels, A., Xia, Y., Bex, V., Midgley, P.M. (Eds.), Climate Change 2013: the Physical Science Basis. Contribution of Working Group I to the Fifth Assessment Report of the Intergovernmental Panel on Climate Change. Cambridge University Press, Cambridge, United Kingdom and New York, NY, USA, p. 1535. https://doi.org/10.1017/CBO9781107415324.

IPCC, 2021. In: Masson-Delmotte, V., Zhai, P., Pirani, A., Connors, S.L., Péan, C., Berger, S., Caud, N., Chen, Y., Goldfarb, L., Gomis, M.I., Huang, M., Leitzell, K., Lonnoy, E., Matthews, J.B.R., Maycock, T.K., Waterfield, T., Yelekçi, O., Yu, R., Zhou, B. (Eds.), Climate Change 2021: the Physical Science Basis. Contribution of Working Group I to the Sixth Assessment Report of the Intergovernmental Panel on Climate Change. Cambridge University Press (in press). https://www.ipcc.ch/report/ar6/wg1/.

Karion, A., Lopez-Coto, I., Gourdji, S.M., Mueller, K., Ghosh, S., Callahan, W., Stock, M., DiGangi, E., Prinzivalli, S., Whetstone, J., 2021. Background conditions for an urban greenhouse gas network in the Washington, DC, and Baltimore metropolitan region. Atmos. Chem. Phys. 21 (2021), 6257–6273. https://doi.org/10.5194/acp-21-6257-2021.

Lac, C., Donnelly, R.P., Masson, V., Pal, S., Riette, S., Donier, S., Queguiner, S., Tanguy, G., Ammoura, L., Xueref-Remy, I., 2013. CO_2 dispersion modelling over Paris region within the CO_2-MEGAPARIS project. Atmos. Chem. Phys. 13, 4941–4961. https://doi.org/10.5194/acp-13-4941-2013.

Lauvaux, T., Miles, N.L., Deng, A., Richardson, S.J., Cambaliza, M.O., Davis, K.J., Gaudet, B., Gurney, K.R., Huang, J., O'Keefe, D., Song, Y., Karion, A., Oda, T., Patarasuk, R., Razlivano, I., Sarmiento, D., Shepson, P., Sweeney, C., Turnbull, J., Wu, K., 2016. High-resolution atmospheric inversion of urban CO_2 emissions during the dormant season of the Indianapolis Flux Experiment (INFLUX). J. Geophys. Res. 121 (10), 5213–5236.

Lelandais, L., Xueref-Remy, I., Riandet, A., Sauvage, S., Blanc, P.E., Delmotte, M., Ramonet, M., Armengaud, A., 2022. Analysis of 6.5 years of atmospheric CO_2, CH_4, CO continuous observations (2014-2020) and their correlations, at the Observatoire de Haute Provence, France a station of the ICOS-France national greenhouse gases observation network. Atmos. Environ. (in press).

Lemonsu, A., Pigeon, G., Masson, V., Moppert, C., 2006. Sea-town interactions over Marseille: 3D urban boundary layer and thermodynamic fields near the surface. Theor. Appl. Climatol. 84, 171–178. https://doi.org/10.1007/s00704-005-0155-y.

Lopez, M., Schmidt, M., Yver, C., Messager, C., Worthy, D., Kazan, V., Ramonet, M., Bousquet, P., Ciais, P., 2012. Seasonal variation of N_2O emissions in France inferred from atmospheric N_2O and Rn^{222} measurements. J. Geophys. Res. Atmos. 117, D14103 https://doi.org/10.1029/2012JD017703.

Lopez, M., Schmidt, M., Delmotte, M., Colomb, A., Gros, V., Janssen, C., Lehman, S.J., Mondelain, D., Perrussel, O., Ramonet, M., Xueref-Remy, I., Bousquet, P., 2013. CO, NO_X and $^{13}CO_2$ as tracers for fossil fuel CO_2: results from a pilot study in Paris during winter 2010. Atmos. Chem. Phys. 13, 7343–7358. https://doi.org/10.5194/acp-13-7343-2013.

Lopez-Coto, I., Ren, X., Salmon, O.E., Karion, A., Shepson, P.B., Dickerson, R.R., Stein, A., Prasad, K., Whetstone, J.R., 2020. Wintertime CO2, CH4, and CO emissions estimation for the Washington, DC–baltimore metropolitan area using an inverse modeling technique. Environ. Sci. Technol. 54 (5), 2606–2614. https://doi.org/10.1021/acs.est.9b06619, 2020.

Mahesh, P., Sharma, N., Dadhwal, V.K., Rao, P.V.N., Apparao, B.V., Ghosh, A.K., Mallikarjun, K., Ali, M.M., 2014. Impact of land-sea breeze and rainfall on CO_2 variations at a coastal station. J. Earth Sci. Climatic Change 5 (201), 6. https://doi.org/10.4172/2157-7617.1000201.

Martin, C.R., Zeng, N., Karion, A., Mueller, K., Ghosh, S., Lopez-Coto, I., Gurney, K.R., Oda, T., Prasad, K., Liu, Y., Whetstone, J., 2019. Investigating sources of variability and error in simulations of carbon dioxide in an urban region. Atmos. Environ. 199, 55–69. https://doi.org/10.1016/j.atmosenv.2018.11.013.

Mestayer, P.G., Durand, P., Augustin, P., Bastin, S., Bonnefond, J.M., Bénech, B., Campistron, B., Coppalle, A., Delbarre, H., Dousset, B., Drobinski, P., Druilhet, A., Fréjafon, E., Grimmond, C.S.B., Groleau, D., Irvine, M., Kergomard, C., Kermadi, S., Lagouarde, J.P., Lemonsu, A., Lohou, F., Long, N., Masson, V., Moppert, C., Noilhan, J., Offerle, B., Oke, T.R., Pigeon, G., Puygrenier, V., Roberts, S., Rosant, J. M., Saïd, F., Salmond, J., Talbaut, M., Voogt, J., 2005. The urban boundary-layer field campaign in Marseille (UBL/CLU-ESCOMPTE): set-up and first results, Bound.-Layer. Meteorol. 114, 315–365. https://doi.org/10.1007/s10546-004-9241-4.

Miller, S.T.K., Keim, B.D., Talbot, R., Mao, H., 2003. Sea breeze: structure, forecasting, and impacts. Rev. Geophys. 41 (3), 1011. https://doi.org/10.1029/2003RG000124.

Nasrallah, H.A., Balling Jr., R.C., Madi, S.M., Al-Ansari, L., 2003. Temporal variations in atmospheric CO_2 concentrations in Kuwait City, Kuwait with comparisons to Phoenix, Arizona, USA. Environ. Pollut. 121, 301–305. https://doi.org/10.1016/S0269-7491(02)00221-X.

Nathan, B.J., Lauvaux, T., Turnbull, J.C., Richardson, S.J., Miles, N.L., Gurney, K.R., 2018. Source sector attribution of CO_2 emissions using an urban CO/CO_2 bayesian inversion system. J. Geophys. Res. 123 (23), 13611–13621. https://doi.org/10.1029/2018JD029231.

Pal, S., Xueref-Remy, I., Ammoura, L., Chazette, P., Gibert, F., et al., 2012. Spatio-temporal Variability of the Atmospheric Boundary Layer Depth over the Paris Agglomeration: an Assessment of the Impact of the Urban Heat Island Intensity, vol. 63. Atmosph. Env., Elsevier, pp. 261–275. https://doi.org/10.1016/j.atmosenv.2012.09.046.

Pérez-Landa, G., Ciais, P., Gangoiti, G., Palau, J.L., Carrara, A., Gioli, B., Miglietta, F., Schumacher, M., Millan, M.M., Sanz, M.J., 2007. Mesoscale circulations over complex terrain in the Valencia coastal region, Spain – Part 2: modeling CO_2 transport using idealized surface fluxes. Atmos. Chem. Phys. 7, 1851–1868. https://doi.org/10.5194/acp-7-1851-2007.

Puygrenier, V., Lohou, F., Campistron, B., Saïd, F., Pigeon, G., Bénech, B., Serça, D., 2005. Investigation on the fine structure of sea-breeze during ESCOMPTE experiment. Atmos. Res. 74, 329–353. https://doi.org/10.1016/j.atmosres.2004.06.011.

Rayner, P.J., Raupach, M.R., Paget, M., Peylin, P., Koffi, E., 2010. A new global gridded data set of CO_2 emissions from fossil fuel combustion: methodology and evaluation. J. Geophys. Res. 115, D19306 https://doi.org/10.1029/2009JD013439.

Rice, A., Bostrom, G., 2011. Measurements of carbon dioxide in an Oregon metropolitan region. Atmos. Environ. 45, 1138–1144. https://doi.org/10.1016/j.atmosenv.2010.11.026.

Ritchie, H., Roser, M., 2020. CO_2 and greenhouse gas emissions, published online at OurWorldInData.org. retrieved from. https://ourworldindata.org/co2-and-other-greenhouse-gas-emissions. https://ourworldindata.org/co2-and-other-greenhouse-gas-emissions [Online Resource].

Rolph, G., Stein, A., Stunder, B., 2017. Real-time environmental applications and display sYstem: READY. Environ. Model. Software 95, 210–228. https://doi.org/10.1016/j.envsoft.2017.06.025.

Schmidt, M., Lopez, M., Yver Kwok, C., Messager, C., Ramonet, M., Wastine, B., Vuillemin, C., Truong, F., Gal, B., Parmentier, E., Cloué, O., Ciais, P., 2014. High-precision quasi-continuous atmospheric greenhouse gas measurements at Trainou tower (Orléans forest, France), Atmos. Meas. Tech. 7, 2283–2296. https://doi.org/10.5194/amt-7-2283-2014.

Seto, K.C., Dhakal, S., Bigio, A., Blanco, S., Delgado, G.C., Dewar, D., Huang, L., Inaba, A., Kansal, A., Lwasa, S., McMahon, J.E., Müller, D.B., Murakami, J., Nagendra, H., Ramaswami, A., 2014. Human settlements, infrastructure and spatial planning. In: Edenhofer, O., Pichs-Madruga, R., Sokona, Y., Farahani, E., Kadner, S., Seyboth, K., Adler, A., Baum, I., Brunner, S., Eickemeier, P., Kriemann, B., Savolainen, J., Schlömer, S., Von Stechow, C., Zwickel, T., Minx, J.C. (Eds.), Climate Change 2014: Mitigation of Climate Change. Contribution of Working Group III to the Fifth Assessment Report of the Intergovernmental Panel on Climate Change. Cambridge University Press, Cambridge, United Kingdom and New York, NY, USA.

Staufer, J., Broquet, G., Bréon, F.M., Puygrenier, V., Chevallier, F., Xueref-Remy, I., Dieudonné, E., Lopez, M., Schmidt, M., Ramonet, M., Perrussel, O., Lac, C., Wu, L., Ciais, P., 2016. The first 1-year-long estimate of the Paris region fossil fuel CO_2 emissions based on atmospheric inversion. Atmos. Chem. Phys. 16, 14703–14726. https://doi.org/10.5194/acp-16-14703-2016.

Stein, A.F., Draxler, R.R., Rolph, G.D., Stunder, B.J.B., Cohen, M.D., Ngan, F., 2015. NOAA's HYSPLIT atmospheric transport and dispersion modeling system. Bull. Am. Meteorol. Soc. 96, 2059–2077. https://doi.org/10.1175/BAMS-D-14-00110.1.

Stull, R.B., 1988. Mean boundary layer characteristics. In: Stull, R.B. (Ed.), An Introduction to Boundary Layer Meteorology, Atmospheric Sciences Library, vol. 13. Springer, Dordrecht. https://doi.org/10.1007/978-94-009-3027-8_1.

Stunder, B.J.B., 1996. An assessment of the quality of forecast trajectories. J. Appl. Meteorol. 35 (8), 1319–1331.

Turnbull, J.C., Sweeney, C., Karion, A., Newberger, T., Lehman, S.J., Tans, P.P., Davis, K. J., Lavaux, T., Miles, N.L., Richardson, S.J., Cambaliza, M.O., Shepson, P.B., Gurney, K., Patarasuk, R., Razlivanov, I., 2015. Toward quantification and source sector identification of fossil fuel CO_2 emissions from an urban area: results from the INFLUX experiment. J. Geophys. Res. Atmos. 120, 292–312. https://doi.org/10.1002/2014JD022555.

Turnbull, J.C., Karion, A., Davis, K.J., Lauvaux, T., Miles, N.L., Richardson, S.J., Sweeney, C., McKain, K., Lehman, S.J., Gurney, K.R., Patarasuk, R., Liang, J., Shepson, P.B., Heimburger, A., Harvey, R., Whetstone, J., 2018. Synthesis of urban CO_2 emission estimates from multiple methods from the Indianapolis flux project (INFLUX). Environ. Sci. Technol. 53 (1), 287–295. https://doi.org/10.1021/acs.est.8b05552, 2019.

United Nations, 2019. World Urbanization Prospects: the 2018 Revision. the United Nations, New York, p. 126. https://population.un.org/wup/Publications/Files/WUP2018-Report.pdf.

Verhulst, K.R., Karion, A., Kim, J., Salameh, P.K., Keeling, R.F., Newman, S., Miller, J., Sloop, C., Pongetti, T., Rao, P., Wong, C., Hopkins, F.M., Yadav, V., Weiss, R.F., Duren, R.M., Miller, C.E., 2017. Carbon dioxide and methane measurements from the Los Angeles Megacity Carbon Project – Part 1: calibration, urban enhancements, and uncertainty estimates. Atmos. Chem. Phys. 17, 8313–8341. https://doi.org/10.5194/acp-17-8313-2017.

Vermeulen, A.T., Hensen, A., Popa, M.E., van den Bulk, W.C.M., Jongejan, P.A.C., 2011. Greenhouse gas observations from cabauw tall tower (1992–2010). Atmos. Meas. Tech. 4, 617–644. https://doi.org/10.5194/amt-4-617-2011.

Wimart-Rousseau, C., Wagener, T., Raimbault, P., Lagadec, V., Lafont, M., Garcia, N., Lajaunie-Salla, K., Diaz, F., Pinazo, C., Yohia, C., Garcia, C., Xueref-Remy, I., Blanc, P.E., Lefèvre, D., 2020. Temporal variability of the carbonate system and air-sea CO_2 exchanges in the bay of Marseille (North Western Mediterranean Sea) over a two-year period (2016-2018). J. Estuarine coastal shelf sci. 236 https://doi.org/10.1016/j.ecss.2020.106641.

Wolf Jr., C., Dalal, S., DaVanzo, J., Larson, E.V., Akhmedjonov, A., Dogo, H., Huang, M., Montoya, S., 2011. China and India, 2025: a Comparative Assessment. RAND Corporation, Santa Monica, CA, USA.

Xueref-Remy, I., Dieudonné, E., Vuillemin, C., Lopez, M., Lac, C., Schmidt, M., Delmotte, M., Chevallier, F., Ravetta, F., Perrussel, O., Ciais, P., Bréon, F.-M., Broquet, G., Ramonet, M., Spain, T.G., Ampe, C., 2018. Diurnal, synoptic and seasonal variability of atmospheric CO_2 in the Paris megacity area. Atmos. Chem. Phys. 18, 3335–3362. https://doi.org/10.5194/acp-18-3335-2018.